Original

Ignjatović, S.; Blawert, C.; Serdechnova, M.; Karpushenkov, S.; Damjanović, M.; Karlova, P.; Wieland, D.C.F.; Starykevich, M.; Stojanović, S.; Damjanović-Vasilić, L.; Zheludkevich, M.L.:
Formation of multi-functional TiO2 surfaces on AA2024 alloy using plasma electrolytic oxidation.
In: Applied Surface Science. Vol. 544 (2021) 148875.

First published online by Elsevier: 26.12.2020

https://dx.doi.org/10.1016/j.apsusc.2019.144552

Applied Surface Science 544 (2021) 148875

Contents lists available at ScienceDirect

Applied Surface Science

journal homepage: www.elsevier.com/locate/apsusc

Full Length Article

Formation of multi-functional TiO_2 surfaces on AA2024 alloy using plasma electrolytic oxidation

S. Ignjatović [a], C. Blawert [b], M. Serdechnova [b,*], S. Karpushenkov [c], M. Damjanović [a], P. Karlova [b], D.C.F. Wieland [b], M. Starykevich [d], S. Stojanović [e], Lj. Damjanović-Vasilić [e], M. L. Zheludkevich [b,f]

[a] Chemical Agrosava, Krnješevačka bb, 22310 Šimanovci, Serbia
[b] Institute of Materials Research, Helmholtz-Zentrum Geesthacht, Max-Planck-Straße 1, 21502 Geesthacht, Germany
[c] Belarusian State University, Faculty of Chemistry, Nezavisimosti Avenue 4, 220030 Minsk, Belarus
[d] Department of Materials and Ceramic Engineering, CICECO - Aveiro Institute of Materials, University of Aveiro, 3810-193 Aveiro, Portugal
[e] University of Belgrade, Faculty of Physical Chemistry, Studentski trg 12-16, 11000 Belgrade, Serbia
[f] Institute for Materials Science, Faculty of Engineering, University of Kiel, Kaiserstraße 2, 24143 Kiel, Germany

ARTICLE INFO

Keywords:
Plasma electrolytic oxidation
Multifunctional coatings
AA2024 alloy
Titanium dioxide
Corrosion and wear resistance

ABSTRACT

Plasma electrolytic oxidation (PEO) was applied to functionalise the surface of AA2024 alloy. A potassium titanium-oxide oxalate dihydrate based aqueous electrolyte was used, which allowed the direct formation of a TiO_2 surface layer on the aluminium alloy substrate. The effect of PEO treatment time and the additional presence of anatase particles in the electrolyte solution on the surface layer and its properties (corrosion, wear and photocatalytic activity) were investigated.

It was found that the coating thickness and surface morphology are strongly dependent on the PEO processing time. However, the phase composition is not much affected by the treatment time and the main coating phase is rutile with a smaller amount of anatase. Adding additional anatase in the form of particles increases the amount of anatase in the coatings. The additional particle addition has only minor effect on the corrosion resistance, but reduces the wear resistance remarkably. Interestingly, the addition of anatase particles and the PEO treatment time are not effective in increasing the photocatalytic activities of the samples.

1. Introduction

Plasma electrolytic oxidation, also known as micro arc oxidation or anodic spark deposition is a surface engineering technology, which is considered to be one of the most cost-effective and environmentally friendly ways to produce stable oxide coatings on the surface of light-weight metals (aluminium, magnesium, titanium, etc.) and their alloys.

The main constituents of the PEO coating are high-temperature oxide phases, which are synthesized inside the dielectric discharge channels out of substrate and electrolyte species. This is possible due to high local temperatures and instantaneous plasma formation, which lead to rapid heating and cooling of the oxide layer [1–8]. Such coatings consist of not only substrate metal oxides, but also products of physicochemical transformations of electrolyte components under the effect of electrical discharges. The latter makes it possible to influence directly the composition and properties of coatings by varying the electrolyte composition [9–12].

In the PEO formation process, the ceramic coating growth takes place at the sites of the micro-discharges, as it grows inwards to the alloy substrate and outwards to the coating surface simultaneously. For the coating growth, there are three simultaneous processes taking place: the electrochemical reactions, the plasma chemical reactions and thermal diffusion, which makes PEO coating growth mechanism a complex process. Over the last decade, significant progress has been made in both the understanding and utilization of the plasma in order to obtain coatings with desired properties, as well as understanding the micro-discharge phenomena and the coating growth mechanisms [6,8,13–16]. The coating microstructure and phase composition are typically a result of the discharges [6,15]. Rapid localized heating is quickly cooled by the electrolyte, which leads to production of a mixture of high-temperature crystalline and amorphous oxide phases. With the additional influence of electrolyte and substrate a large variety of

* Corresponding author. Tel.: +49 4152 87 1991; fax: +49 4152 87 1960.
E-mail address: maria.serdechnova@hzg.de (M. Serdechnova).

https://doi.org/10.1016/j.apsusc.2020.148875
Received 12 September 2020; Received in revised form 23 December 2020; Accepted 26 December 2020
Available online 31 December 2020

different coating compositions exist [17], but it is quite difficult to produce pure oxide coatings different from the substrate metal material.

For example, specific coatings obtained by the PEO process can improve the electrical insulation properties of the metal alloy surface beside offering wear and corrosion resistance [1–6,13,18–26]. Such possibilities to add additional functionalities and to create multi-functional surfaces are getting more and more into the focus of research. TiO_2 coatings combine good chemical stability, tribological properties and photocatalytic activity [27–31]. Titania exists in the form of different polymorphs, but the most common forms are the anatase and rutile crystal structures. Anatase exhibits a higher photocatalytic activity compared to rutile, while rutile is characterized with better tribological properties and stability [32]. The difficulty is to adjust the ratio of the two polymorphs, as anatase tends to transform to rutile at temperatures higher than 600 °C [33]. Titania coatings obtained by PEO processing have been widely investigated [34,35] due to their potential applications, such as biocompatible materials, structural ceramics, photocatalysts or optical coatings. However, TiO_2 is the most widely used photocatalyst, because it is quite stable even in harsh environments, in spite of allowing only the degradation of organic pollutants under UV light irradiation, due to its relatively wide band gap (~3.2 eV for anatase form) [27,28].

Application of TiO_2 layers on Ti alloys and to produce functionalised PEO coatings is well established. The formation of TiO_2 was reported for PEO treatment of titanium alloys, mostly Ti-6Al-4V, for biomedical applications in prosthetic implants [36–38] and photocatalytic applications [31,39]. However, there are only a few studies about the formation of TiO_2 layers on other substrates such as an aluminium surface by PEO [30,40,41,63]. The formation of pure TiO_2 coatings by PEO on Al based substrates is a big challenge. Mostly, TiO_2 is added directly to the electrolytes in form of particles in order to produce Al_2O_3/TiO_2 or mixed oxide/TiO_2 coatings, depending on the electrolyte composition and processing conditions. The coatings offered high hardness, excellent wear and corrosion properties, as well as high thermal resistance or photocatalytic activity. The TiO_2 particles immersed in the electrolyte contributed also to lower porosity of the coatings [41], but pure TiO_2 coatings are not obtained on aluminium substrates.The later was also observed using potassium titanyl oxalate as a low concentrated additive to a silicate based electrolyte [63]. Considering applications like wastewater cleaning it can be interesting to fix the photocatalytic active substance on sheets for easier handling (compared to powders which have to be separated by filtering from the cleaned water). To have a lighter and cheaper sheet substrate is also interesting, thus if aluminium is used instead of titanium. However, the direct deposition/formation of almost pure TiO_2 layers on Al without the use of particles was reported only once to the knowledge of the authors [42]. Latter approach required an aqueous solution containing tetraethyl orthotitanate, acethylacetone, isopropanol and Agitan® as an antifoaming agent. The components except Agitan® are flammable and acethylacetone is toxic. Thus, the idea of present study is to create a TiO_2 coating on Al, but using a simpler and easier to handle electrolyte. From previous works, it was known that a simple aqueous solution of 40 g/L potassium titanium-oxide oxalate dihydrate is a suitable electrolyte for PEO processing of Al [43], but up-to now no detailed study about coating formation and properties was performed. Therefore, in the present study the influence of treatment time was studied to understand if functionalised PEO coatings on Al alloys could be produced with this electrolyte. Furthermore, it was studied if the addition of anatase particles directly to the electrolyte could influence the rutile to anatase ratio in the coating.

2. Experimental

2.1. Material, electrolyte and setup

Rectangular samples of 2024 Al alloy (3.8–4.9% Cu, 0.35–0.5% Fe, 0.1% Cr, 1.2–1.8% Mg, 0.3–0.9% Mn, 0.5% Si, 0.1–0.15% Ti, 0.25% Zn, 0.15% others and Al balance) of 30 mm in length, 20 mm in width and 1,5 mm in thickness were subjected to the PEO treatment. PEO treatments were carried out using a laboratory rig, which consists of a Hameg analogue oscilloscope HM400 40 MHz, a self-made pulse generator and a 3000 W EA-PS 8720-15 DC power supply. The samples were treated for 2.5, 5, 10 and 15 min in constant current mode by applying 50 mA/cm^2 and a pulse ratio of $t_{on} : t_{off} = 1$ ms : 9 ms.

For the treatments the samples were immersed in an aqueous standard electrolyte containing 40 g/L of potassium titanium-oxide oxalate dihydrate ($K_2[TiO(C_2O_4)_2]\cdot 2H_2O$). The starting pH and the conductivity of the electrolyte were 2.7 and 13.3 mS/cm, respectively. The same treatments were repeated with addition of 5 g/L anatase particles (Sigma-Aldrich, TiO_2, 99.8% anatase powder of 200 nm average single particle size, agglomerated to an average size of 1 μm but not bigger than 5 μm (Fig. 1)) to the base electrolyte. In both cases, compressed air bubbling and a cooling system kept the electrolyte and particle dispersion homogenous and its temperature at 20 ± 0.1 °C during the whole process.

There was concern about the stability of the electrolyte, because already after the first treatment a change in colour from clear to yellow in combination with a strong increase of the pH value from 2.7 to 4.7 was observed for the electrolyte. As consequence, the pH was monitored throughout the full set of treatments (40 in total; 5 treatments for each time with and without particles) and the obtained coating thickness was measured for each specimen directly after the treatment (Fig. 2). There was no renewal of the electrolyte and the full set of 40 treatments was performed in the same electrolyte except the addition of 5 g/L anatase particles after 20 treatments. The strong increase of pH became weaker, but throughout the full set of treatments, there was an increasing trend for the pH with some recovery after longer treatment breaks. During this monitoring and during the post-characterisation, there was no indication that the observed electrolyte changes had influenced the treatment result. There are larger thickness variations at longer treatment times, but without a clear trend related to the pH. It is likely, that the colour change is related to the formation of pertitanic acid in the electrolyte according to the following reactions (1) and (2) [44]:

$$[TiO(C_2O_4)_2]^{2-} \rightarrow TiO^{2+} + 2\ C_2O_4^{2-} \quad (1)$$

$$TiO^{2+} + H_2O_2 \rightarrow [TiOH_2O_2]^{2+} \quad (2)$$

However, the equilibrium is obviously more on the side of the TiO-oxalate. Latter is still available for the coating forming process as a negatively charged ion, which is attracted towards the surface during the PEO processing. Both oxalic and pertitanic acid are relatively weak acids and may recombine with H^+ resulting in the observed increase of

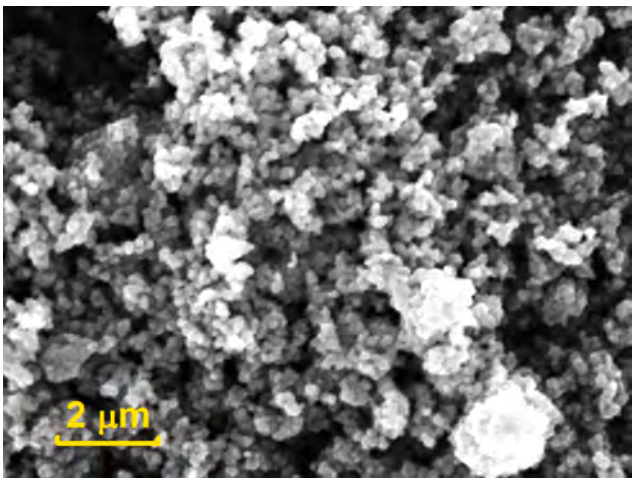

Fig. 1. SEM micrograph of the anatase powder used in the experiments.

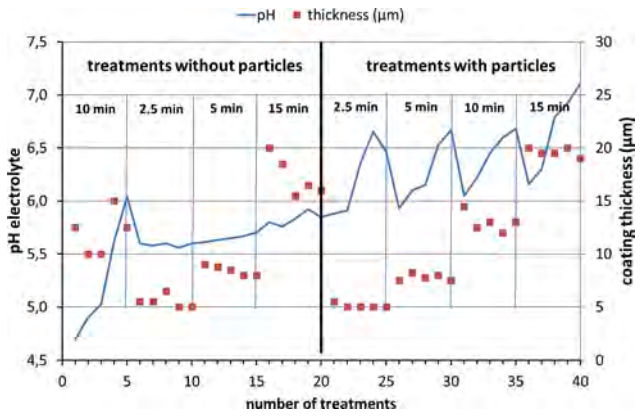

Fig. 2. pH value of the electrolyte as a function of number of treatments performed and thickness of the coating as indicator of reproducibility of the treatment.

the pH.

Because H_2O_2 was not added directly to the electrolyte, it must be assumed that it forms as a side product in the discharges, which is likely as OH radicals are quite often observed in optical emission spectra recorded during PEO processing [45–47] and they may recombine to H_2O_2. The presence of the yellow $[TiOH_2O_2]^{2+}$ complex in the treatment solution was cross check by a decolourisation due to fluoride addition (reaction 3):

$$[TiOH_2O_2]^{2+}{}_{(yellow)} + 6F^- + 2H^+ \rightarrow [TiF_6]^{2-}{}_{(clear)} + H_2O_2 + H_2O \quad (3)$$

2.2. Coating characterization

2.2.1. SEM/EDS

Scanning electron microscope (Vega 3, Tescan, Brno, Czech Republic) equipped with energy dispersive X-ray (EDS) spectrometer (EDS, Heidenrod, Germany) were used to observe surface morphology of the coatings, and to evaluate porosity distribution across the surface. N650 plano-carbon was applied to the surface of the specimens prior to observation, in order to prevent surface charging effects. The specimens were observed using secondary electron and backscattered electron detectors. Furthermore, the cross sections of selected coatings (10 min with/without anatase) were studied and elemental mapping was performed to visualise the distribution of the elements in the layer. For preparation of the cross sections normal metallographic preparation techniques, including cutting, grinding and polishing were applied.

2.2.2. Thickness measurement

After PEO treatment the samples were rinsed with water and dried in air. For non-destructive thickness measurements, a thickness gauge (MiniTest 2100, Elektro Physik, Germany) was used. A minimum of 10 measurements were taken randomly on the surface to calculate the average values.

2.2.3. X-Ray diffraction

The integral phase composition of the coatings was analyzed by applying X-ray diffraction (XRD), using a Bruker D8 Advance diffractometer with a Ni filtered Cu K_α radiation source. A step size of 0,02° and a scan range from 10° to 80° in 2θ scan mode was used, with a glancing angle of 3° and a scan speed of 0.5 s per step. For X-ray generation, a voltage of 40 kV and a current of 40 mA was used.

The coating's crystallographic structural composition and the local distribution were studied at PETRA III (DESY, Hamburg, Germany) at the nano focused endstation of P03 beamline [48] with an X-ray energy of 19.7 keV and a beam size of 1.5 μm by 1.5 μm. The interface region was investigated by performing a mesh scan with a size of 80 per 80 μm with a step size of 2 μm and 4 μm, in perpendicular and lateral directions, respectively. An Eiger 9 M detector (pixel size 75 by 75 μm) with an acquisition time of 0.5 sec for each measuring point was used. Data averaging was done by the software package P*yFAI* [49]. 2θ values of each diffraction pattern was recalculated to Cu K_α radiation for easier comparison with the integral diffraction results.

2.2.4. Glow discharge optical emission spectroscopy

Glow discharge optical emission spectroscopy (GDOES) depth profile analysis of the coatings was conducted with a HORIBA GD-Profiler 2 instrument. A standard 4 mm copper tube anode was used for this purpose, with an anode to sample gap of 0.1 mm. Argon was used as the plasma gas, at operating conditions of 650 Pa pressure and 30 W power. No special sample preparation method was used prior to the analysis, neither was any residue contaminant removing method applied.

2.2.5. Electrochemical impedance spectroscopy

The corrosion resistance of the PEO coated specimens was evaluated by applying electrochemical impedance spectroscopy (EIS) using a computer controlled potentiostat (Interface1000, Gamry), as well as Echem Analyst software (Gamry) for analysis of the data. A sample surface of 0.5 cm^2 was exposed to 330 ml of unstirred 3.5% NaCl corrosive solution, prepared with deionised water.

Tests were carried out in an electrochemical cell using a standard three-electrode setup consisting of an Ag/AgCl (saturated KCl) reference electrode, a Pt counter electrode and the PEO coated specimen as the working electrode. The measurements were performed at room temperature. In order to exclude external interferences, the cell was kept in a Faraday cage while the tests were running. The impedance spectra were recorded after 1, 3, 6, 12, 24, 48, 96 and 168 h from the moment the specimens were exposed to the solution. The potentiostatic EIS tests at open circuit potential (OCP) were set with an initial frequency of 100 kHz and a final frequency of 50 mHz, with an amplitude of ±10 mV. For comparison, the bare surface of the aluminium alloy was subjected to the same test.

2.2.6. Photocatalytic activity

The photocatalytic activities of all samples were tested by measuring the degradation of methyl orange (MO) [27]. The experiment was performed in a glass cell with 10 ml aqueous solution of 8 mgL^{-1} MO under constant stirring (400 rpm) and illumination. The catalyst (specimen surface) was settled on a perforated holder (the same dimension as the sheet, and 4 mm of height) with a magnetic stirrer beneath it. To keep the reaction solutions at room temperature (25 °C), the photocatalytic reactor was equipped with water circulation system. In order to attain adsorption-desorption equilibrium, the catalyst and the solutions were stirred in the dark for 30 min, before illumination. Simulated solar irradiation was carried out using a lamp with an illumination intensity of 16,000 lx (Osram Vitalux 300 W). The lamp was fixed at a distance of 25 cm above the surface of the solution. The total irradiation time was 8 h.

Aliquots (1 ml) were withdrawn every 2 h and the concentration of MO was measured at the maxima (λ = 464 nm) of the absorption spectra. Afterwards the aliquots were taken back to the original solution. UV–Vis spectra of aliquots were collected with a Thermo Scientific Evolution 220 spectrophotometer in the range from 250 to 700 nm. The measured absorbance was converted to concentration in accordance to a standard curve showing a linear relationship between the concentration of MO and the absorbance at the wavelength of 464 nm. In order to examine its stability, prior to the photocatalysis, the MO solution was tested for photolysis in the absence of the photocatalyst. No change in the MO concentration after 8 h of irradiation revealed that it was stable under applied conditions, and that degradation was a result of the presence of the photocatalyst. The degree of MO degradation was given as $((C_0 - C)/C_0)$, where C_0 is the initial MO concentration and C is the concentration of MO after irradiation.

2.2.7. Wear test

The dry sliding wear resistance of the PEO coatings was evaluated using an oscillating wear tester (TRIBO Technic, France). A 5 mm diameter steel ball (100Cr6) was used as counter-part. The sliding distance was 12 m, at a linear velocity of 5 mm/s. The applied loads varied from 3 to 9 N, depending on the specimen to determine the load level at which the coatings fails. A new ball was used for each test.

3. Results

3.1. Voltage – time response

The voltage–time response for PEO of AA2024 alloy in potassium titanium-oxide oxalate dihydrate electrolyte is shown in Fig. 3. Under the driving current density of 50 mA/cm^2, the voltage increased rapidly from the beginning of the oxidation process, reaching 400 V after about 70 s. The nanoparticle additions have relatively minor influences on the voltage – time response and the two curves are overlapping to a large extent.

It is possible to identify four discharge stages in the PEO process, according to the voltage-time curve, as shown in Fig. 3. The stages are distinguished primarily by the change of the slope of the voltage-time curve, but changes in colour, intensity and number of discharges can be noted as well. The discharges start approximately 30 s after the beginning of the PEO process. At first, the micro-discharges are small with a white colour but grow in size and turn yellow/orange at later stages. The size of micro-discharges becomes larger with increasing time of PEO processing, while their population decreases. Generally, as PEO process time increases, the density of micro-discharges decreases, but their intensity and size increase [1]. Many other authors reported a similar PEO process stage classification [6,7,23,47,50–52]:

- Stage I (S1): In this stage similar to conventional anodic oxidation, a sharp increase in voltage can be observed, but the breakdown voltage is not reached yet. It mainly involves the rapid electrochemical formation of an initial insulating oxide film. Decrease in the voltage ramp rate and intensive gas liberation can be observed shortly before the start of discharges.
- Stage II (S2): This stage is characterised by the start of the breakdown of the oxide layer after around 30 s and reaching 300 V. The appearance of first discharges goes together with an increase in temperature and therefore, melting of the substrate surface and an increase in the coating growth rate. The voltage ramp decreases further in this stage, which is visible by micro-arcs increasing in number and covering eventually completely the macroscopic specimen surface.
- Stage III (S3): This stage, where the voltage is increasing slowly, but continuously, comprises the longest treatment period and is characterized by larger but slower moving discharges, which become more intense, but lower in number. The appearance of the micro-discharges in stage III of the process of coating formation is shown in Fig. 4. As the oxide layer grows, its electrical resistance increases and therefore the nature of the plasma changes. Post analysis of the surface morphology also revealed the start of surface discharges due to the presence of bubbles at the surface. By eye, the different discharges are not notable.
- Stage IV (S4): In this stage, the rate of voltage increase is even slower than in stage III. The process becomes more steady state, discharges appear as relatively large, and long lasting sparks, while their population decreases remarkable. However, the occurrence of the strong discharges is less frequent than in stage III due to the thicker coating causing more difficulty in the initiation of such discharges. For some cases, such strong discharges may cause irreversible damage to the coatings in stage IV.

The final voltages recorded after the end of each parameter setting tested are displayed in Table 1. It is obvious that the effect of the particle addition on the voltage-time response can be neglected.

3.2. Coating thickness and oxidation kinetics

The thickness of the coatings with and without anatase particle addition as a function of treatment time is shown in Fig. 5a. The overall coating thickness reached after 15 min is about 17 ± 2.5 μm in the standard electrolyte and with the addition of anatase, it is about 19 ± 0.5 μm. The average growth rate of the coating in the standard electrolyte decreases from an average of 2.2 μm/min in the beginning of the treatment to 1.2 μm/min after 10 min, as shown in Fig. 5b. After 15 min, the growth rate is still around 1.2 μm/min. The calculated growth rates in each time interval (0–2.5 min; 2.5–5 min; 5–10 min; 10–15 min) indicate that a steady state is not reached (Fig. 4b). The growth rate drops to 0.7 μm/min between five and ten minutes before it is increasing again for the last interval to 1.1 μm/min. This can indicate a change in the growth mechanism.

For the PEO treatment with 5 g/L anatase addition, the differences in coating thickness are small compared to the standard electrolyte. However, the average coating growth rate varies from 2.05 μm/min at the beginning to 1.3 μm/min at longer treatment times (Fig. 5b). Thus, anatase addition seems to reduce the growth rate in the earlier stages of the process, while it is increasing the growth rate at longer processing times (Fig. 5b). The coating growth rate calculated for each time interval shows that there is similar behaviour at the beginning of the treatment (from 0 to 2.5 and from 2.5 to 5 min) regardless if particles are present or

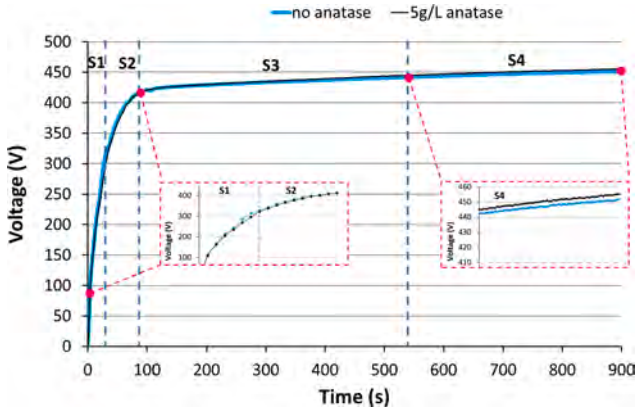

Fig. 3. Voltage-time response for PEO process with and without anatase addition.

Fig. 4. Intense micro-discharges on surface of the metal alloy substrate during PEO processing in stage III.

Table 1
Final voltages after each treatment time.

Electrolyte parameters	Treatment time (min)	Final voltage (V)
40 g/L without anatase	2.5	426.0 ± 3.0
40 g/L with 5 g/L anatase		426.4 ± 1.5
40 g/L without anatase	5	433.6 ± 2.3
40 g/L with 5 g/L anatase		434.4 ± 2.7
40 g/L without anatase	10	444.4 ± 2.6
40 g/L with 5 g/L anatase		440.1 ± 2.7
40 g/L without anatase	15	454.7 ± 2.2
40 g/L with 5 g/L anatase		451.6 ± 3.3

not. However, there is less reduction (only to 1 μm/min) of the growth rate in the interval between 5 and 10 min and a more significant increase to 1.4 μm/min in the final interval if particles are present (Fig. 5b) indicating that particles play a more important role in the later stages of the treatment.

3.3. Surface morphology and coating microstructure

Fig. 6 a-d shows the surface morphologies of the coatings prepared in the standard and anatase containing electrolyte for different treatment times. It is clearly visible, that the coatings have quite different surface morphologies after the different treatment times.

The surface shows a large amount of pores that are remains of "solidified" discharge channels and entrapped bubbles of the gases that are generated during the process. Please note that we are considering the solidified discharge channels as one part of the overall porosity of the coatings. During plasma discharges, processes including melting and re-solidification continuously occur in the outer layer, causing a repetitive fluctuation in surface temperature. The molten ceramic components cool down rapidly in contact with the electrolyte and the gas and vapours dissolved in it will be trapped while the coating is formed. The micro-discharges are generated by a dielectric breakdown at thin/weak coating areas, thus, passing the PEO. The number of those sites is reduced as the coating thickness increases e.g. by longer treatment times. Thus, there is more energy required for a single discharge. As a consequence, the size of the discharge channels is increasing and, therefore, the size of the visible open porosity.

Pores of different sizes and shapes were observed on all the coated samples. Micro-pores of diameters less than 5 μm are visible on the surface of the initial stage of the PEO process, and are a characteristic of such ceramic coatings (Fig. 6). The majority of the open pores in the early stages have a size of around 1 μm. Shorter processing times yield the highest density of open pores, see Fig. 6. Increasing the treatment time reduce the number of the pores remarkably, but they seem to grow in size. They reach maximum diameters of around 10 μm after 10 and 15 min of PEO processing.

The coating surfaces are generally consisting of three types of morphologies, as presented in Fig. 7: (I) a significant part of the surface is covered with crater-like microstructures formed by micro-discharge events, (II) nodular structures and (III) cracks. The cratered areas are usually composed of oxidized titanium and contain discharge channels in the form of central holes through which molten and/or evaporated material flowed out of the channel to rapidly solidify and create distinctive boundaries of solidified craters. Similar observations were reported by other authors [1]. The melt volume is obviously quite low and not much mixing occurs between the dense oxide barrier layer and the top TiO_2 coating even if discharges are passing through the coating (Fig. 8 a-b). However, there is a second type of bigger craters (size of around 40 μm in diameter), which do not have this centre discharge channel, suggesting that they may form via discharges occurring between surface and electrolyte maybe via gas phase (gas bubble sticking on the surface). Similar round structures were observed also during PEO processing with PTFE particles in the electrolyte [53].

The surface morphologies of the coatings prepared with 5 g/L anatase addition for different treatment times are presented in Fig. 6 e-h. The change of the overall surface morphology with increasing treatment time is very similar compared to the standard electrolyte. In general, the pores seem to decrease in number, but grow in size as the treatment time is increasing.

The presence of the added anatase particles can be seen in Fig. 9. The particles seem to be inert and do not react with the coating phases while they are deposited on the surface of the coating (most likely by sticking in melt pools). The same crater-like structures as observed for the pure electrolyte are present at the surface. The bigger craters appear to be slightly increased in size, from approximately 40 μm to around 50 μm, possibly due to a change of electrolyte viscosity due to the particle addition changing the size of bubbles sticking on the surface.

Representative cross sections and the elemental mappings of the 10 min treated specimens in the standard electrolyte and with the addition of anatase are shown as an example in Fig. 8c. The SEM micrographs show for both synthesis conditions a coating, which can be separated into two regions consisting of the main coating and a well-defined interface layer with a thickness of around 1.5 ± 0.5 μm. This layer contains Al, Ti and O suggesting that it consists of mixed oxides of Al_2O_3 and TiO_2. Looking in more detail and considering the contrast, the interface layer consists of two layers. A darker inner almost perfectly dense layer (Al_2O_3) and a lighter obviously more mixed layer (Al_2O_3 + TiO_2) on top of it are separated by a dashed pore band (Fig. 8 a,b). The main coating is free of Al (at least below the detection limit) and contains only Ti and O (TiO_2). The thickness is around 7 ± 4 μm, which is quite consistent with the non-destructive gauge measurements. The coating, which is grown in the presence of anatase has some particle inclusions which are mainly located in pores (which are in the submicron size).

3.4. Phase composition

The XRD results of the PEO specimens treated in the different

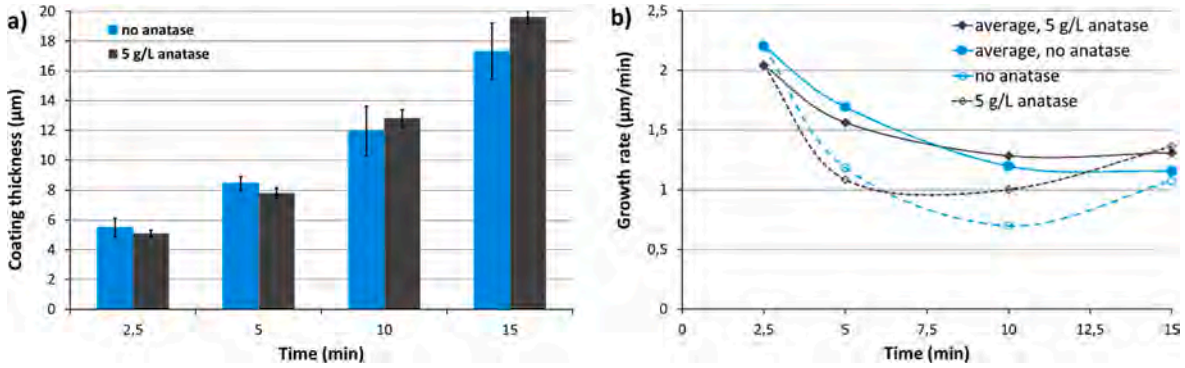

Fig. 5. PEO coating thickness (x) as function of treatment time (t) (a) and respective coating growth rates – average (x/t_{Total}) and $\Delta x/\Delta t$ (b).

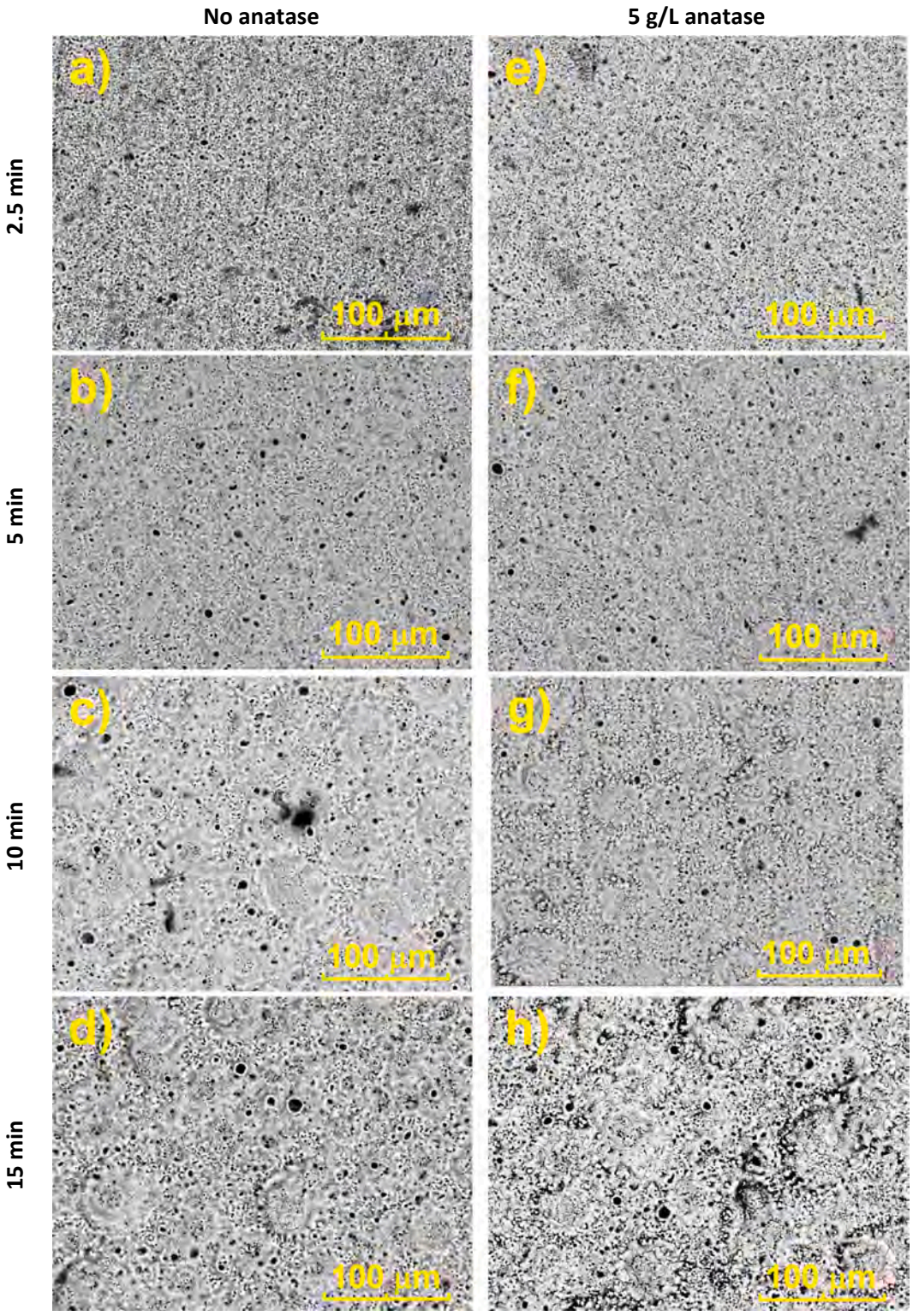

Fig. 6. SEM micrographs showing surface morphology of PEO coatings produced without (a-d) and with (e-g) anatase addition and different treatment times – (a, e) 2.5 min; (b, f) 5 min; (c, g) 10 min; (d, h) 15 min.

conditions are shown in Fig. 10.

With increasing treatment time the coating thickness is increasing, which is indicated by the reduced intensity of the aluminium substrate peaks. The coating itself is composed of anatase and rutile, while the latter is the dominating phase. The rutile crystals seems to have a preferential orientation in the coating, as the expected (1 1 0) peak at 27.3° [54] is not the strongest peak, but the (1 0 1) peak at 36°. In the case of the standard electrolyte the ratio between anatase and rutile is changing with treatment time. Dividing the intensities of the strongest rutile peaks (1 0 1) at 36° by the intensities of the strongest anatase peaks (1 0 1) at 25.2° [55], the highest amount of anatase is reached at 5 min treatment time and with increasing time the ratio becomes larger again (Fig. 11). With longer treatment times, there is obviously a decreasing amount of anatase compared to rutile present in the coating.

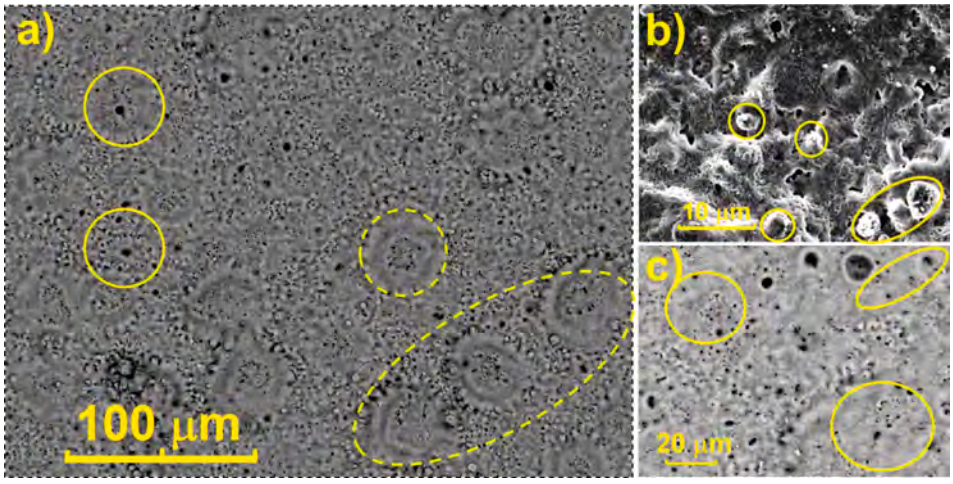

Fig. 7. Surface morphology obtained from the 10 min standard specimen: (a) two types of craters – based on discharge channels across the coating marked by solid line and based on surface discharges around gas bubbles sticking on the surface marked by dashed line; (b) nodular structures and (c) cracks.

After the addition of 5 g/L anatase particles to the electrolyte (Fig. 10b), the same trend, as it was observed for the pure electrolyte, could be visible. The highest amount of anatase was obtained after 5 min treatment, reaching almost the same amount as rutile. In general, the amount of anatase is higher in the coating as compared to the standard electrolyte (Fig. 11). In addition, the negative effect by prolonging treatment time is weakened.

There seems to be an effective increase of anatase in the coating by the up-take of anatase particles from the electrolyte. However, it seems to be possible that longer treatment times and higher final voltages (higher energy in the discharges) are leading to a partial conversion of the anatase particles to rutile, but on the other hand larger pore size should allow additional up-take of particles. To learn more about the distribution of the two TiO_2 phases within the coating high resolution, localised XRD scans through the coating were performed at the beamline P03, PETRAIII (DESY). Fig. 12 shows such a scan from the surface towards the interface. It is quite interesting to observe that the anatase content in the coating produced in the standard electrolyte is quite low and that it can be increased remarkably due to the anatase addition. Surprisingly, the highest concentration of anatase is at the interface towards the substrate and not at the surface, suggesting that the particles are incorporated mainly via fast pathways such as open pores. Furthermore, a mixed oxide Al_2TiO_5 can be found in a narrow region of the interface, which was hardly seen in the integral XRD measurements. This observation confirms the findings of the elemental mappings of the cross sections. We note that the coatings appear to be thicker compared to gauge measurements and cross sections. This can be due to a real thickness increase as the measurement was done on the edge to have a region, which is consisting of 100% coating and by an artificial increase due to measuring geometry. Latter can be influenced by roughness of the coating, by a rounded shape of the coating at the edge and a slight tilt of the sample within the holder.

3.5. Elemental depth distribution

In addition, elemental depth profiles were recorded with special focus on the Al distribution to assess the purity of the TiO_2 top layer. The results obtained by GDOES show that there are four main regions, which can be identified within the PEO coatings (Fig. 13). The regions are basically defined by the Ti and O signals and their change of slope. Region I corresponds to the top PEO layer and shows strong titanium and oxygen signals. There is almost no Al at the surface, especially for the longer treatment times. From the XRD results and the SEM cross sections, it can be concluded that the TiO_2 forms rutile and anatase in this region. After the top layer, a region of mixed oxides based on Ti and Al is visible (zone II), partly $TiAl_2O_5$ according to the localised high-resolution XRD measurements. This mixed oxide layer is richer in Ti_2O close to the surface and richer in Al_2O_3 closer to the interface with the substrate. In the following transition region (zone III) the intensity of aluminium signal starts increasing remarkably, while the intensity of titanium signal decreases and reaches almost zero at the end of the transition region. Zone III indicates that the PEO layer and substrate alloy are sputtered at the same time. The transition from zone I/II to zone IV (alloy substrate) is not sharp. Thus, it is likely that the coating is not uniform in thickness, that the interface between coating and substrate is rough or that different distribution of phases in the coating lead to different sputter rates. Region IV is the substrate and is characterized by high levels of base alloy elements, such as copper, and mostly aluminium.

Compared to the standard electrolyte the addition of the anatase particles has no remarkable effect on the zones of the depth profiles. The same regions are visible and the already observed slowing down effect on the growth rate of the coating in the earlier stages of PEO coating formation and the enhancing effect at longer treatment durations is confirmed.

3.6. Corrosion behaviour

The electrochemical impedance spectroscopy results (Bode plots) for selected PEO coatings (2.5 and 15 min) produced in the standard electrolyte after immersion for 1, 3, 6, 12, 24, 48, 96 and 168 h in 3.5% NaCl are shown in Fig. 14. For comparison, the EIS results of bare Al sample are also shown. The time dependent degradation of all coatings is shown in Fig. 15.

As expected, the starting impedance modules of all coated specimens are much higher than the one for the uncoated substrate in full frequency range. Although the values of all coated samples decrease over time, they are still higher at the end of the tests after 168 h. The 2.5 min sample treated in the standard electrolyte shows the highest impedance modulus values at low frequencies throughout the whole test (Figs. 14 and 15). As $|Z|$ at low frequencies correlates in a certain way with the corrosion resistance, it means that the 2.5 min sample demonstrates an improved corrosion resistance. In the 1 h measurement the $|Z|$ value was around $2{\cdot}10^7$ Ωcm^2, which is considerably higher compared to all the other specimens treated in the standard electrolyte and it decreased only to approximately $2{\cdot}10^5$ Ωcm^2 after 168 h immersion.

All thicker specimens from the standard electrolyte have a starting $|Z|$ value of approximately $5{\cdot}10^5$ Ωcm^2 and decrease only slightly after 1 h of immersion (Fig. 15). The corrosion resistance of the 5 min specimen remains quite stable during the full immersion period. It decreases

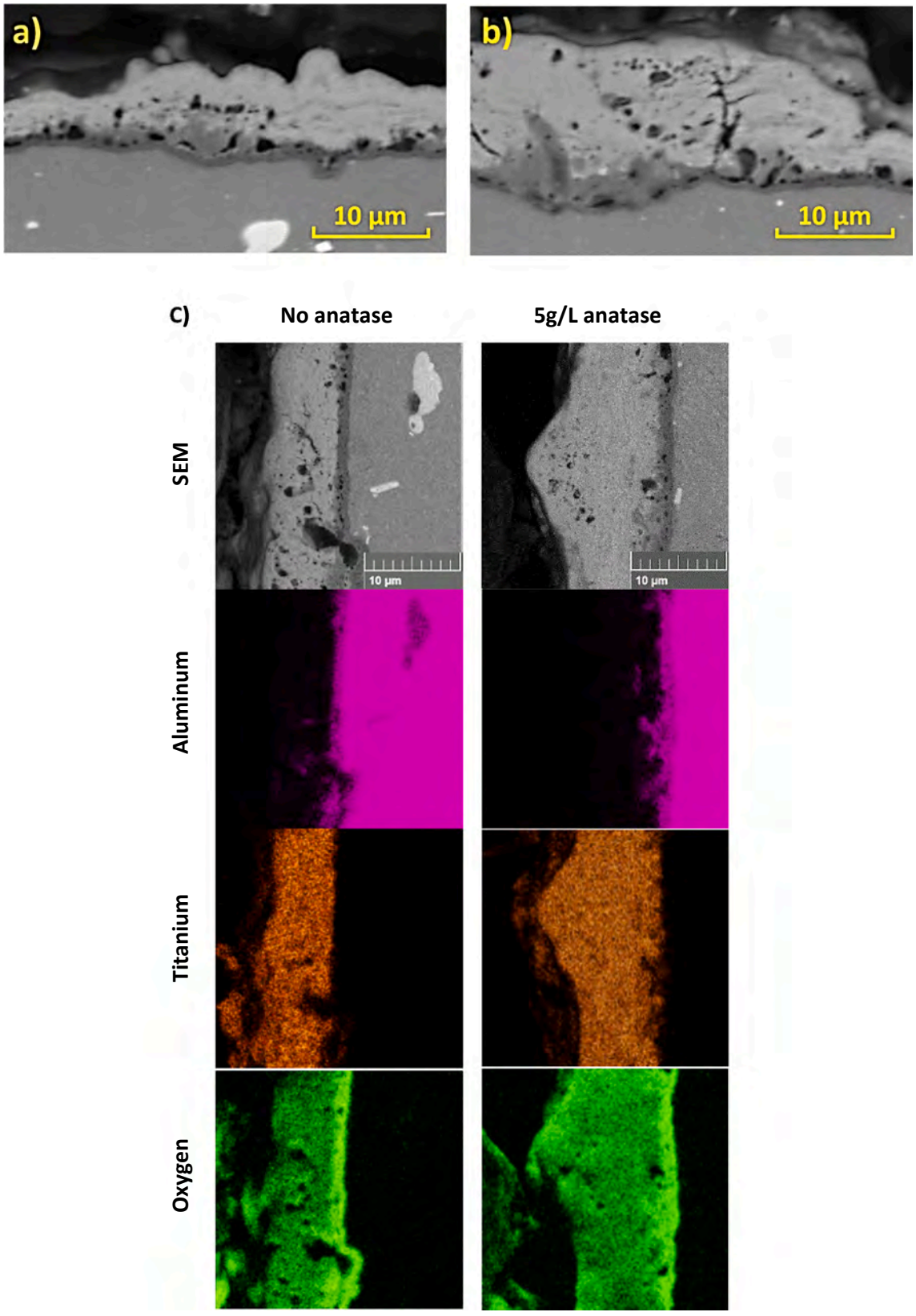

Fig. 8. Cross-sections of two selected regions of the 10 min treated coatings a) standard (no anatase); b) 5 g/L anatase addition and c) elemental mapping of two different regions of the 10 min standard and 5 g anatase samples.

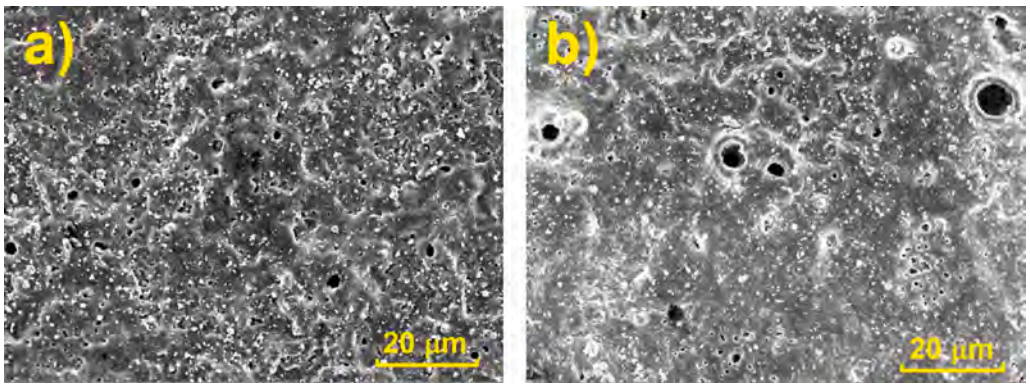

Fig. 9. Anatase particles deposited on the surface of the specimen – (a) 5 g/L anatase 5 min sample; (b) 5 g/L anatase 15 min sample.

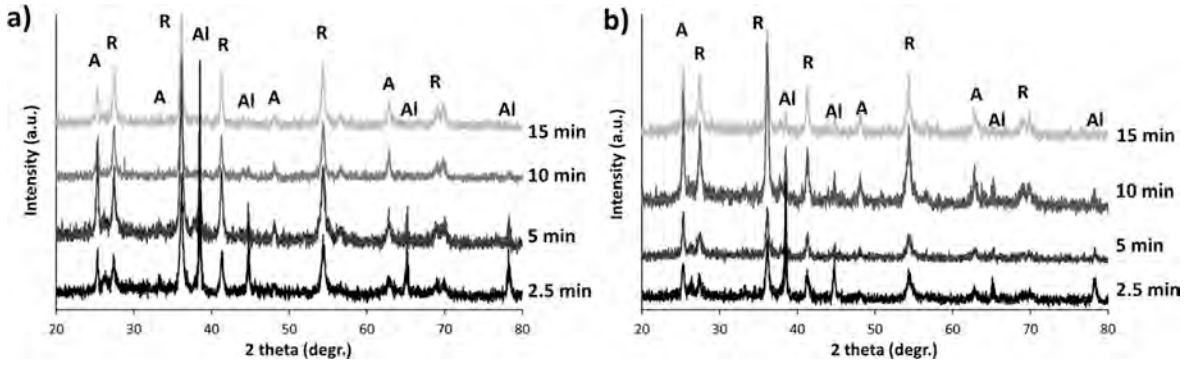

Fig. 10. XRD results of a) PEO coatings without Anatase – 2.5, 5, 10, 15 min treatment time and b) PEO coatings with 5 g/L Anatase particle addition – 2.5, 5, 10, 15 min treatment time. "R" indicates rutile, "A" – anatase, "Al" – AA2024 substrate.

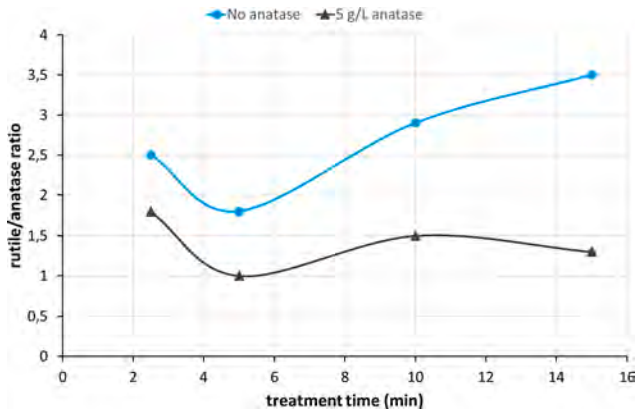

Fig. 11. Rutile to anatase ratio as a function of treatment time and anatase particle addition to the electrolyte calculated from the XRD measurements using the intensities of rutile (1 0 1) and anatase (1 0 1) peaks. Lines are just a guidance for the eye.

slightly in the beginning to a |Z| of around 10^4 Ωcm^2 and recovers to 10^5 Ωcm^2 at the end of the test. The 10 min sample was able to maintain its low frequency |Z| value of around 10^5 Ωcm^2 until 24 h of immersion. From 48 h on the |Z| value drops continuously and reaches $2.4{\cdot}10^4$ Ωcm^2 after 168 h. The 15 min specimen also demonstrates an excellent corrosion resistance with a |Z| value above 10^5 Ωcm^2 throughout the whole test. At the end, the impedance was still at around 10^5 Ωcm^2.

Similar to the results of the specimens produced in the standard electrolyte, the impedance modulus values of all samples with particle addition decrease over time (Figs. 14 and 15). The 2.5 min sample, once again, shows the highest impedance modulus values at the beginning of the test, but it degrades faster compared to the specimens produced in the standard electrolyte. In the 1 h measurement the |Z| value was around $1.5{\cdot}10^7$ Ωcm^2, which is by an order of magnitude higher compared to all the other specimens and it decreased to roughly $8{\cdot}10^4$ Ωcm^2 after 168 h immersion, which is almost one order lower than the specimens treated for 10 and 15 min. In the 12 and 24 h measurement, the coating seems to have recovered in a certain way, as it shows impedance values of approximately $3{\cdot}10^6$ Ωcm^2.

The 5 min sample showed a |Z| value at low frequencies of around $6{\cdot}10^5$ Ωcm^2 after 1 h of immersion, dropping below $1{\cdot}10^5$ after 3 h and further to $4{\cdot}10^4$ Ωcm^2 after 168 h (Fig. 15). The specimens that have been subjected to the PEO process for 10 and 15 min have a starting |Z| value in the range of $1{\cdot}10^6$–$3{\cdot}10^6$ Ωcm^2 after 1 h immersion. The 10 min sample demonstrates very good stability of corrosion resistance as its |Z| value drops continuously throughout the whole test to only slightly less than $1{\cdot}10^6$ Ωcm^2 after 168 h immersion, so it is characterized with the lowest |Z| value drop from the beginning to the end of the test. The same could be noted for the 15 min sample, as it was able to maintain its impedance values higher than $1{\cdot}10^6$ Ωcm^2 until 48 h of immersion, to drop only to slightly below $1{\cdot}10^6$Ωcm^2 after 168 h.

Certain similarities in the EIS results between the standard and 5 g/L anatase specimens can be observed, especially for the 2.5 and 15 min samples (Fig. 14), which are both attributed with good corrosion protection properties. In both cases, the 2.5 min sample |Z| value at low frequencies starts from roughly $2{\cdot}10^7$ Ωcm^2, which are the highest starting values compared to the other specimens, but the degradation of the coating is faster. The 15 min samples in both cases are characterized with the smallest |Z| value drop, meaning they were able to maintain decent corrosion protection throughout the whole test. Looking at the differences between the specimens with or without particle addition (Fig. 15), the 5 g anatase samples show generally higher starting impedance values at low frequencies compared to the standard

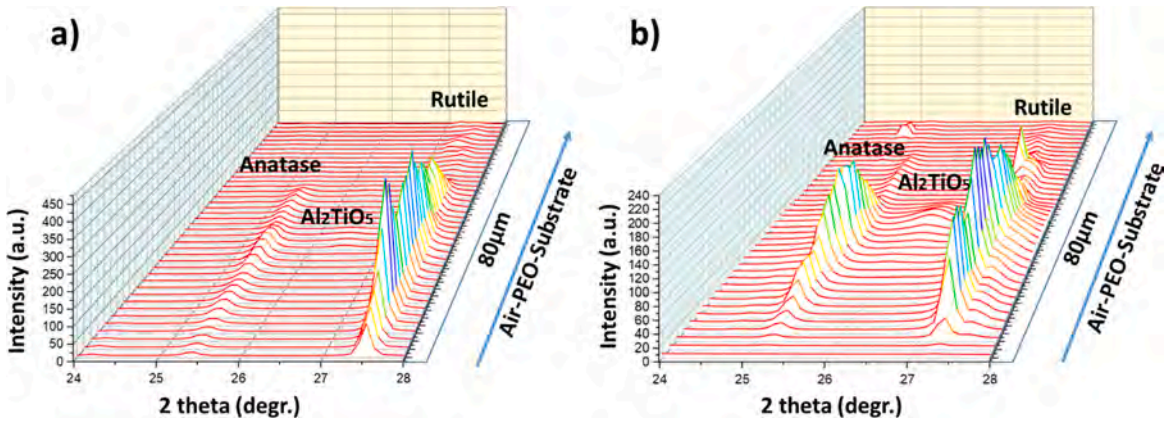

Fig. 12. Rutile and anatase phase distribution across the coating thickness demonstrated by the intensity of (1 1 0) rutile and (1 0 1) anatase XRD peaks for a) 10 min treatment; 0 g anatase addition b) 10 min treatment; 5 g/l anatase addition. Distance between each measurement is 2 µm and intensities are not normalized.

specimens, as well as higher values at the end of the tests especially for the 10 and 15 min samples. Thus to summarize, it can be stated, that the corrosion resistance of the specimens is improved due to the particle addition.

3.7. Photocatalytic activity

Fig. 16a shows the rate of degradation of methyl orange as a function of time for the different coatings produced in the standard electrolyte. Surprisingly, there is no trend visible. The best photocatalytic activity was observed for the coating that was treated for 10 min, showing that 25.7% of the original MO was degraded. The worst result was obtained for the coating treated for 15 min, degrading only 9.4% of MO after 8 h. The 2.5 min and 5 min specimens were able to degrade 17.3% and 15.5% of MO, respectively.

The influence of the anatase addition is shown in Fig. 16b. The specimens treated for 2.5 min and 5 min revealed the best performance with 22% and 21.8% of MO degraded, respectively. The 10 min and 15 min specimens were able to degrade 10% and 17.6% of the total MO concentration.

From these results, it is obvious that the treatment time is not an essential parameter when it comes to photocatalytic activity. The addition of 5 g/L of anatase increased the photocatalytic activity of all specimens, except for the sample treated for 10 min. Out of all specimens, the 10 min sample produced in the standard electrolyte showed the best photocatalytic activity. It seems as if the concentration of anatase directly at the surface is the most influencing parameter, but from the results it is difficult to correlate the concentration with treatment time or the addition of anatase particles.

3.8. Wear behaviour

The wear tests were performed with increasing loads to identify the load bearing capacity of the coatings. Fig. 17 shows, as an example, the changes of the friction coefficients (*fc*) as a function of time for the specimens prepared in standard electrolyte and with anatase particle addition to demonstrate the two possible cases when coating survives or fails. There is a running in period observed in each test when the friction coefficient is increasing with time, which is most likely due to increasing contact area due to increasing wear of the ball and the coating. The *fc* is rather low (less than 0.2) at the beginning of the tests, and then has a sudden increase to around 0.6 in the running in period. At the end of the running in period, either the coating fails and the *fc* is dropping down to 0.4 or the coating is surviving, approaching a final stable range of *fc*. All this happens normally within the first 500 s of the test. The average stabilised fc of the coating in contact with the 100Cr6 steel is around 0.7 to 0.8. In the case of a coating defect and AA2024/steel contact the *fc* is around 0.4 with higher fluctuations of the values, because of fretting wear between the two metals. The addition of 5 g/L anatase particles does not significantly affect the *fc* of the coatings.

However, the addition of particles decreases dramatically the load bearing capacity of the coatings (Fig. 18). Interestingly, this occurs in spite of the thicker coatings being formed at longer treatment times. In contrast to the standard electrolyte where an expected increase in load bearing capacity with increasing coating thickness is observed, this is not the case for the particle addition. Regardless of 5, 10 or 15 min treatment time, the coatings do fail all at a relatively low load of 6 N, mostly in less than 100 s after the beginning of the test (Fig. 17).

Fig. 19 display images taken from representative areas found inside the wear tracks formed on the coated samples of different thicknesses that were subjected to different loads. Fig. 19 a-c displays images of wear tracks formed on specimens that could not withstand the load applied, and Fig. 19 d-f shows wear tracks formed on samples that were able to withstand the applied loads.

The average width of the wear tracks seems to increase as a function of the applied load. This can be explained by the fact that the ball and specimen suffered wear and the area of contact increased between them as the applied load increased (Fig. 19). The micrographs in Fig. 19 a-c show the complete removal of the coating in along the wear track leaving the substrate exposed. The substrate experiences a considerable damage by a combination of adhesive (fretting) and abrasive wear. The high stresses generated during the test produce severe plastic deformations in certain regions of the substrate. The thinner brittle coatings with lower load bearing capacity could not follow this deformation and started to crack and being delaminated from the substrate. Those coating flakes are working as a third body in the wear process and accelerates the wear of the substrate (Fig. 20 a). However, when the thickness and load bearing capacity is high enough, the coatings remained adhered to the substrate and the samples show only accumulated debris and wear products from the ball in the wear track (Figs. 19 d-f, 20b). Interestingly, the load bearing capacity is not improved by the particle addition and it might be speculated at this moment that anatase TiO_2 particles sticking at the surface may act as hard relative loose third body particles in the wear process leading to an earlier damage of the coatings. Furthermore, rutile is considered as the more wear resistant phase [32], which may also play a role if the anatase content is increased by the treatment.

Summarising, the best tribological performance was found for the 15 min PEO treatment in the standard electrolyte, with a thickness of approximately 17 µm. Such coatings were able to endure loads of up to 8 N without major damage of the coating. All coatings that were subjected to 9 N loads were removed completely during the wear test. Only small parts of the coating remained adhered to the substrate in some regions of the wear track.

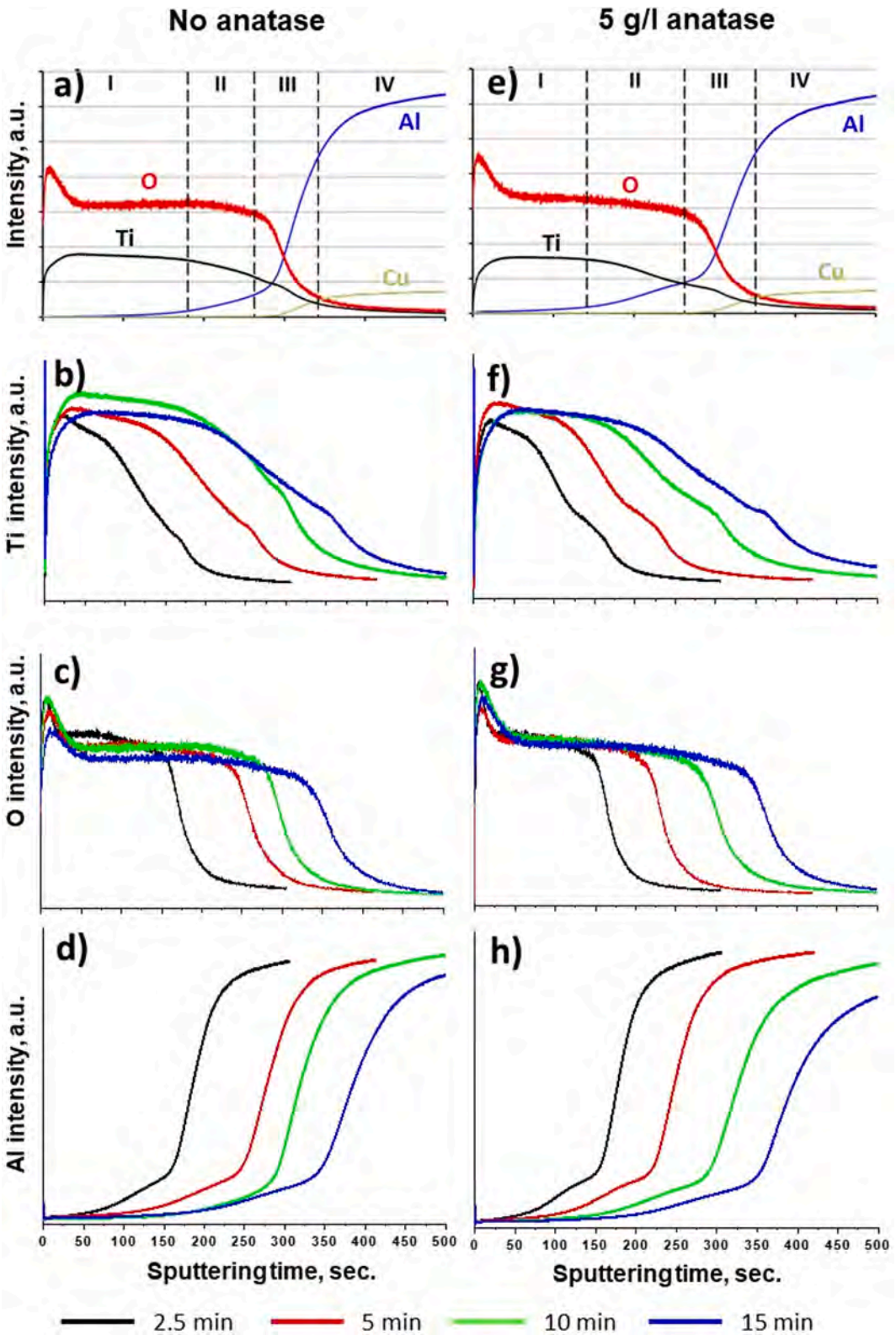

Fig. 13. Qualitative depth profiles measured by GDOES of PEO coated AA2024 – with and without anatase particle addition (example of elemental distribution after 10 min of treatment in the coatings and the respective coating/substrate zones (a, e) and depth distribution of the three main coating forming elements as a function of treatment time (b, f – Ti; c, g – O; d, h – Al).

4. Discussion

The possibilities of plasma electrolytic oxidation, as an environmentally friendly technology with excellent prospects for numerous applications are now widely recognized. The PEO technique has been used to modify the surface of aluminium alloys by producing well-adhered coatings of high hardness, involving micro-arc formation on the work-piece under immersed conditions in a temperature controlled

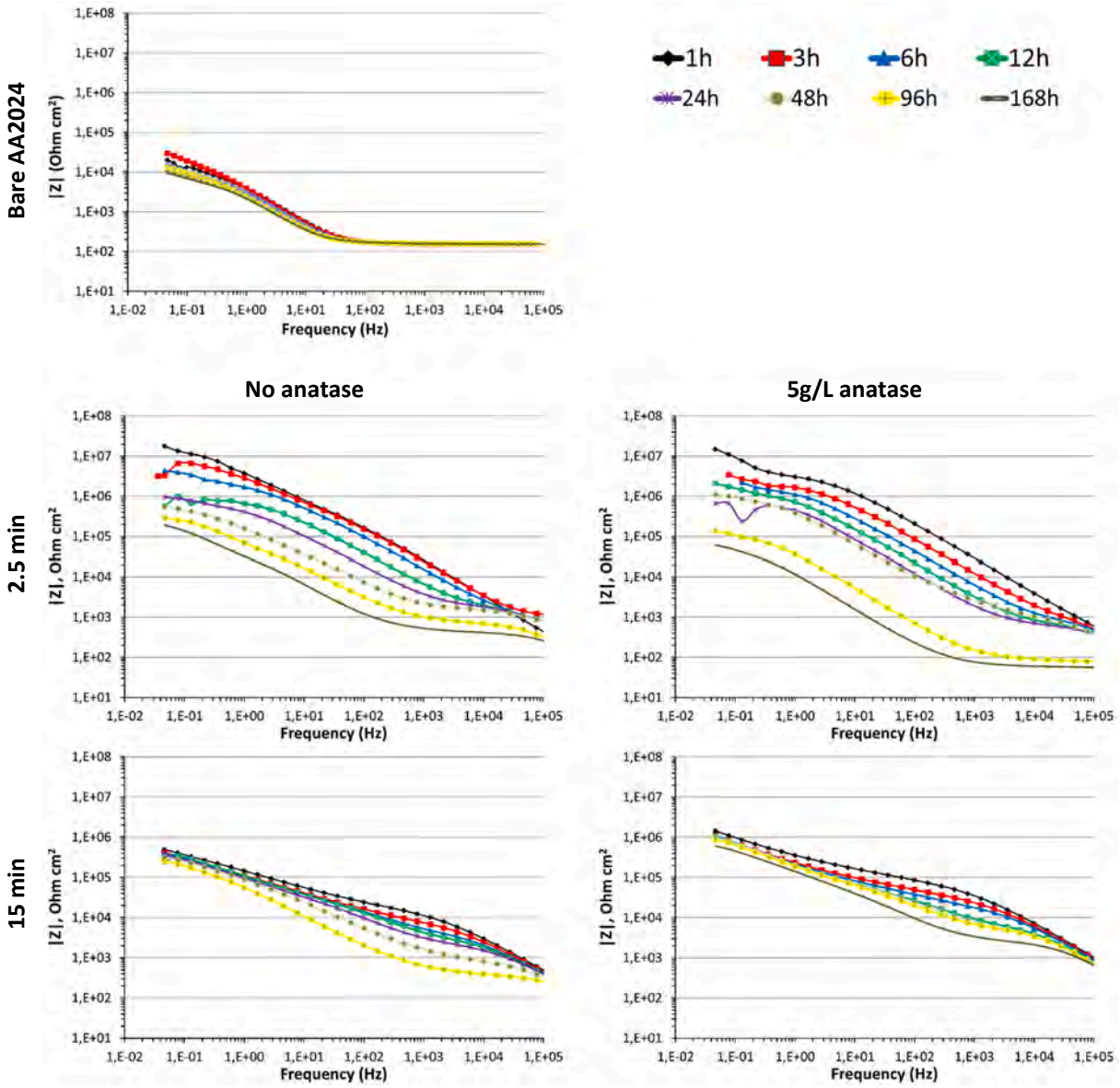

Fig. 14. Electrochemical impedance spectroscopy results (Bode plots) for bare AA2024 alloy as well as PEO coated (2.5 and 15 min) with and without anatase particles additions. The spectra are recorded after 1, 3, 6, 12, 24, 48, 96 and 168 h of immersion.

aqueous electrolyte [13,19,20–22]. Due to the inherent porosity of the coatings, they can be impregnated with functional (e.g. catalytic) particles, which was also used in the present study to extend their possible field of applications. As the PEO treatment time is increasing, the morphologies of the coatings are changing which is obvious and expected (Fig. 6). Three types of different structures can be noticed: pores, craters and nodules. Pores and craters were formed due to melting and resolidification of the surface under the discharges and the related periodical temperature fluctuations, as well as the gases generated in the process, which are solved in the liquid melt and entrapped during solidification. The number of pores and their density decreases with increasing PEO processing time, but the pores grow in size. The thicker the PEO coating is, the bigger is the size of the open craters. This happens due to the higher energy needed for the breakdown of the dielectric barrier of the coating and to create the micro-discharges, which consequently get more intense. However, our data indicates that two kinds of discharges are present. There are those discharges which occur due to a potential difference across the coating and which form the typical crater like open discharge channels. If the processing time is extended to 10 min a second type of discharges occurs which are not destructive for the coating but form large craters without discharge channel in the centre. We assume those originate via a potential difference between the coating surface and isolating gas phase. A similar type of craters was also observed in a previous study of in-situ incorporation of PTFE particles during PEO processing [53]. The crater formation was related to micro bubbles sticking at the surface leading to an increased intensity of the electric field at the edge of the bubbles and facilitating rapid sintering of PTFE particles. Similar behaviour can be expected for the TiO-complexes [$TiO(C_2O_4)_2]^{2-}$ in the case of the present electrolyte. The addition of anatase particles doesn't change too much the discharge behaviour, as obvious from a similar voltage-time response (Fig. 3). Visibly, the open craters are in the same size and number as in the standard electrolyte, which is consistent with similar coating thicknesses and final process voltages. Concerning the second type of "surface" discharges, an earlier occurrence is observed and typical craters are already visible after 5 min treatment. As the anatase particles also contribute to coating formation the formed craters seem to growth a little bit faster compared with the standard electrolyte. Furthermore, the particles influence the viscosity

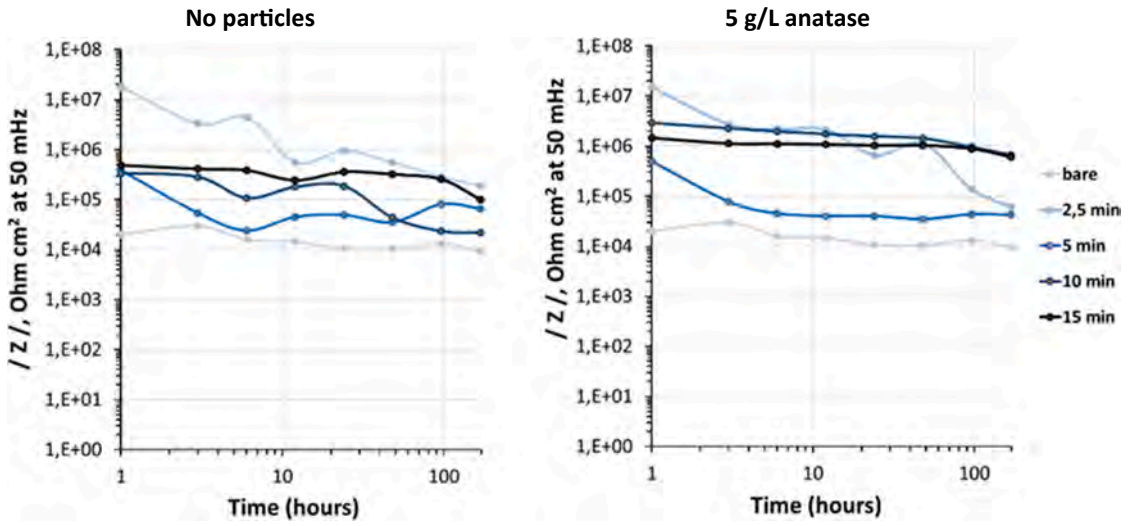

Fig. 15. Evolution of low frequency resistance module (at 50 mHz) as function of immersion time for PEO coatings with different treatment time.

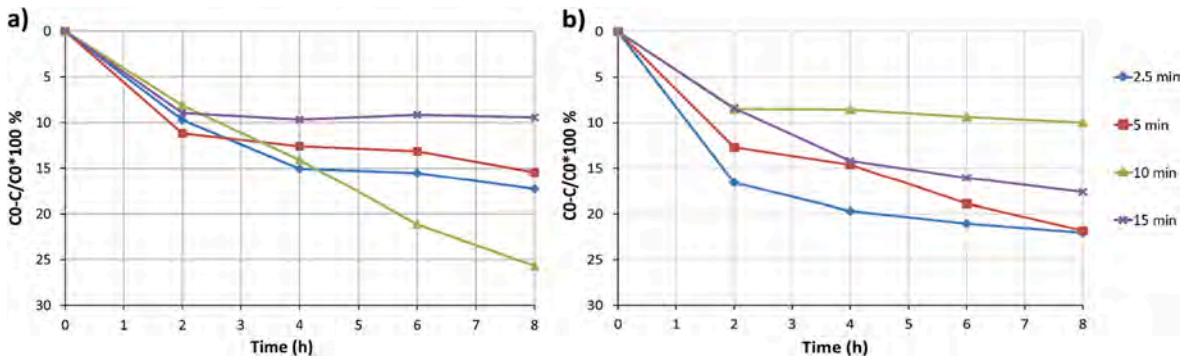

Fig. 16. MO degradation as a function of time for coating produced with a) 0 g anatase and b) 5 g anatase.

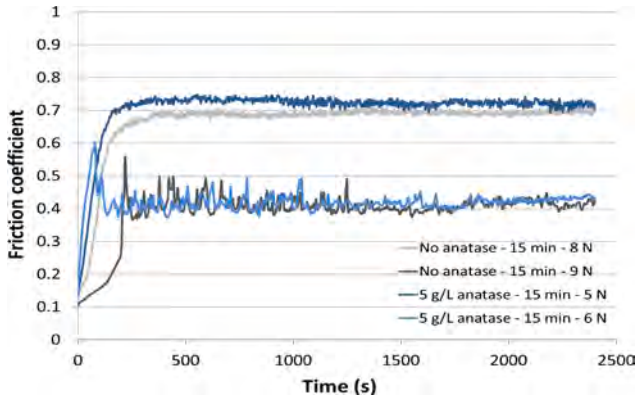

Fig. 17. Friction coefficient as a function of time for specimens that have been treated for 15 min in standard and 5 g anatase electrolyte.

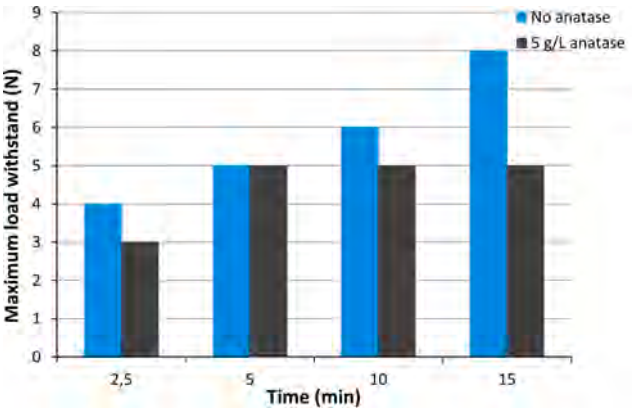

Fig. 18. Comparison of maximum loads applied in the wear tests of standard and 5 g anatase specimens without coating failure.

of the electrolyte and the surface roughness, which in return obviously allows slightly larger bubbles to stick at the surface before they are released to the electrolyte. The consequences are craters, which are forming earlier and which are up to 50 μm in diameter after 15 min of treatment if particles are present.

The thickness of the coatings depends on the treatment time, but there is no linear correlation between treatment time and coating thickness. In the beginning of the PEO process, the average coating growth rate is higher, decreases with time, and may reach a constant steady state value at longer times (10 to 15 min). However, a closer look at the actual growth rates in the respective intervals indicates that there is a minimum growth rate at around 10 min before it is increasing again in the last period. Interestingly, this growth behaviour correlates with the appearance of the second type of discharges. The addition of 5 g/L of anatase particles slowed down the coating formation in the beginning, but at longer periods it contributed to an increase of coating thickness compared to the standard electrolyte. The coating formation seems to be a mixture of a classical PEO growth and an in-situ deposition process. In

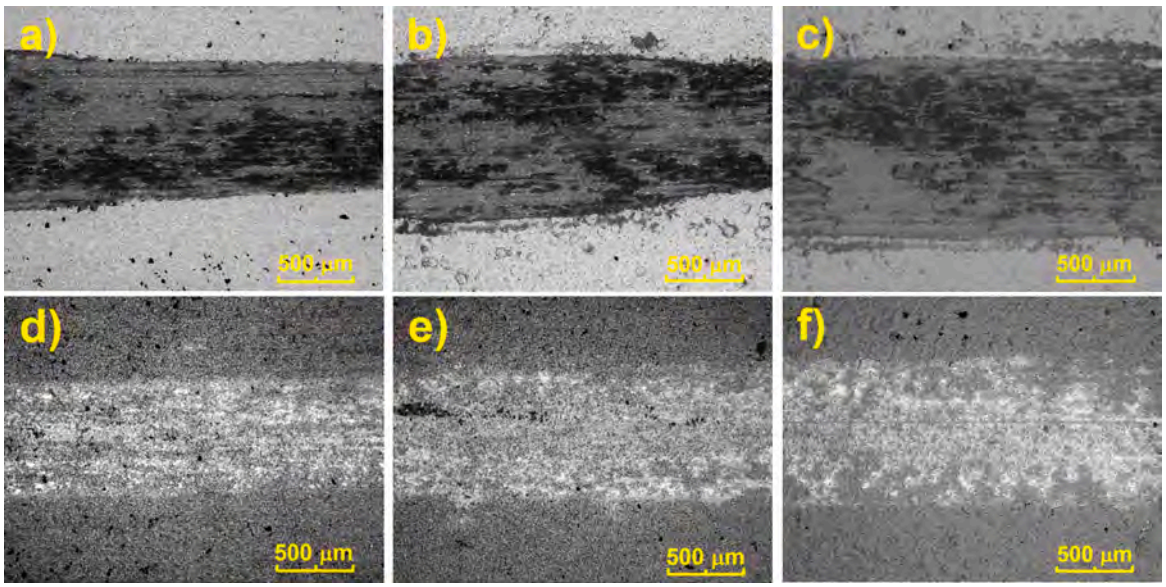

Fig. 19. Wear tracks on samples, which failed the wear test under different loads: a) 5 g anatase – 2.5 min – 4 N; b) 5 g anatase – 15 min – 6 N and c) 0 g anatase – 10 min – 7 N and on samples that passed the wear test under different loads: d) 5 g/L anatase – 2.5 min – 3 N; e) 5 g/L anatase – 5 min – 5 N and f) 0 g anatase – 15 min – 8 N.

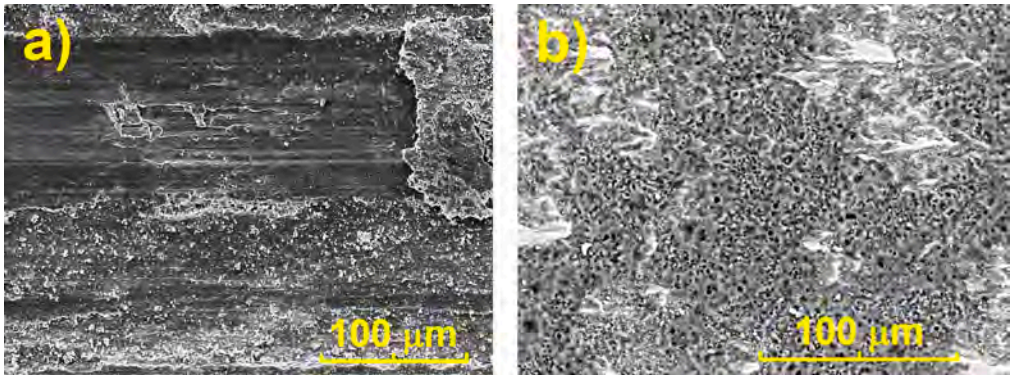

Fig. 20. (a) PEO coating being removed partly and acting as third body particles causing abrasive wear – 5 g/L anatase 10 min sample, 7 N load; (b) Coating remaining adherent with debris and wear products from the ball – no anatase 5 min sample, 5 N load.

the classical PEO process, the coating formation is a result of a combination of substrate and electrolyte compounds reacting and forming the coating. During the in-situ deposition process only components from the electrolyte are deposited and sintered to form the coating. The GDOES depth profiles confirm the existence of 4 zones in the PEO coatings. Zone I represents the surface layer, which is rich in Ti and O. According to the XRD results, this surface layer is TiO_2 and actually a mixture of rutile and anatase depending on the processing parameters. The presence of Ti and absence of Al means that it is formed only from components of the electrolyte. Obviously, it is more a classical deposition process, where the charged TiO-complexes $[TiO(C_2O_4)_2]^{2-}$ are attracted towards the surface, decompose under the discharges conditions and form TiO_2. The repetitive discharges are responsible to sinter the TiO_2 into a relatively dense coating. Thus, it is obviously not the classical PEO formation process, where the coating is composed of parts from the electrolyte and coating at the same time. Here a deposition process of TiO_2 as decomposition product of the potassium titanium-oxide oxalate or another TiO_2 based complex forming in the electrolyte seems to be the main coating formation step. The deposition is stimulated by the discharges, but no extensive mixing of substrate and electrolyte components occurs. There is only a quite thin interface region (zone II) of around 1.5 µm, where both oxides (TiO_2 and Al_2O_3) do appear at the same time (Figs. 8, 12, 13). Probably, the process starts classically with the formation of an Al_2O_3 dielectric layer but with the start of discharges the dominant mechanisms shifts from substrate conversion to deposition out of the electrolyte. An explanation might be that the start of TiO_2 deposition fully blocks the diffusion of Al through the TiO_2 layer just maintaining this relatively sharp border between the two oxide phases. Interestingly, the addition of the particles does not affect the type of zones or the phases forming them, except that the ratio of anatase to rutile and the thickness of the zones can be influenced. This is understandable because oxide particles such as TiO_2 can already develop a negative zeta-potential if they are immersed in slightly acidic electrolytes with the potential getting more negative with increasing pH [56]. Thus, they should behave in a similar manner as the negative charged TiO-oxalate $[TiO(C_2O_4)_2]^{2-}$ in the standard electrolyte. They retard in the beginning the formation of a dense dielectric barrier layer, but later increase the growth rate of the coatings because of a higher concentration of Ti compounds, which form the coating in the deposition controlled coating formation phase. This change of coating growth rate with particle addition was observed with increasing treatment time (Fig. 5). However, it needs further detailed studies to identify the involved mechanisms. The cross sections and the elemental mappings are in agreement with GDOES results (Figs. 8, 12, 13). They demonstrate the highest presence

of Ti in the outer layer (TiO_2) of the coating and of Al in the substrate, with those two elements mixing in the intermediate layer as Al_2TiO_5. Thus, oxygen is present in the outer layer almost purely as TiO_2 and as a mixture of TiO_2 and Al_2O_3 in different ratios in the intermediate layer. The XRD results confirm that the final coating contains mainly TiO_2 in the form of rutile and anatase. In the case of the standard electrolyte, a significantly lower amount of anatase compared to rutile can be noted. Adding 5 g/L anatase particles to the electrolyte was effective in increasing the amount of anatase remarkably. However, the ratio of anatase to rutile phase decreases, with an increase of PEO treatment time, which can be interpreted as a result of polymorphic transformation (starting at around 600 °C) of anatase into rutile at higher PEO energies [33,57].

From the protection perspective, thicker coatings should be more resistant against the penetration of the electrolyte and delay the corrosion process better than thin ones. In practice, in the case of PEO coatings it is not only the coating thickness that determines the corrosion resistance, but also the number of open discharge channels, pores and cracks [58–60]. Thus, some authors report a decrease in the corrosion resistance of thicker layers because of the higher porosity of the ceramic coating, which is a result of the nature of the micro-discharges during PEO process [61]. Others suggest that an increase in the thickness improves the corrosion resistance of the PEO coated material by preventing the electrolyte to penetrate into the inner coating regions [62]. In the present study the latter seems to be true for the long term corrosion behaviour of the thicker coatings prepared at longer treatment times and in the presence of anatase particles, as their corrosion resistance abilities seem to be quite stable over time. This implies that the coatings do have a reduced internal open porosity, which might be related to the blocking of pores by the particles. Due to the combined deposition and discharge processes involved in the coating formation the internal coating porosity is relatively low even at longer treatment times (Fig. 8), increasing the resistance and importance of the outer layer in the overall corrosion performance. However, in the beginning of the testing the thinnest coatings treated for 2.5 min do have the higher resistance values and without particle addition, it even remains the best coating throughout the full 168 h immersion period, although the degradation rate is faster. This good performance is attributed to the denser inner layer of the mixed oxides, which can form a barrier against corrosion of the substrate. Without particle addition, it contains fewer defects as particles are distributed preferentially closer to the interface. This clearly shows that the thickness is not the only dominating factor for the corrosion resistance. However, thickness and porosity (number, size, length and total volume of pores) in the outer TiO_2 layer and the inner mixed oxide barrier layer, determines the diffusivity of the ions through the layers and the time when aggressive ions do reach the substrate. Furthermore, in smaller pore volumes and thicker coatings it is easier to reach favourable conditions of concentration and pH in the coatings, which allows the formation of stable corrosion products blocking the pores if solubility limits of certain compounds are exceeded. In the long term, the thicker samples prepared in 5 g anatase electrolyte showed better corrosion resistance due to the longer diffusion paths within the coating and less pore volume compared to the standard samples.

Regarding the photocatalytic activity, no clear trend is visible. The best performance with degradation of 26% of initial concentration of MO was found for the 10 min treated specimen in the standard electrolyte. With anatase addition the best performance was reached at short treatment times, being able to degrade approximately 22% of initial MO. These results show that the PEO treatment time on the one hand is not essential in sense of increasing photocatalytic activity. The 5 g/L anatase addition generally improved photocatalytic activity, but became worse with longer treatment time. Unfortunately, anatase is not the stable phase and tends to transform to rutile at temperatures around 600 to 700 °C [33]. Such a temperature can be reached easily in the discharges and most of the anatase should actually convert to rutile under the discharges. Thus, this conversion becomes more effective at longer treatment times, because the energy in the discharges is increasing as well as the lifetime of the discharges. At the shorter treatment times, the chance for anatase to survive is higher, but the pores are smaller which makes it difficult for the particles to enter the coating. This brings another aspect into consideration. To be effective the anatase has to be at or close to the surface so that the light can reach it. Anatase is surviving somehow the discharges, even at longer treatment times but looking at the nano-focussed XRD results, the main concentration is closer to the interface with the substrate where it is not effective in photo-degradation. To summarise, it appears to be quite difficult to control what happens with the anatase and where it forms or remains within the coating during the PEO process. However, even a small amount forms under the discharge conditions in the standard electrolyte, which is a surprise because in the discharges the temperatures should be much higher, but it may form during the cooling cycle or the high pressure conditions in the discharge may shift the conditions of its formation.

The wear tests demonstrate that the wear resistance obviously increases with longer PEO treatment times for specimens treated in the standard electrolyte, which is not the case for anatase addition. The poorer performance of the coatings produced in the electrolyte with anatase addition might be explained by the quick occurrence of three body wear. Some anatase particles which are not firmly attached to the surface act as third body hard particles being detrimental for the coating itself and the ball. Furthermore, it has to be considered that rutile is the more wear resistant phase and replacing it partly by anatase might contribute additionally to the poorer wear performance. The width of the wear track increases with heavier loads applied, because wear occurring on both the steel ball and the coating surface is increasing the contact surface area between those two wear partners. Damage of the coating occur, when the PEO coating is too thin and the load bearing capacity of the coating is not high enough to prevent plastic deformation of the substrate underneath. The brittle ceramic-based PEO coating is not able to follow larger plastic deformations and starts to delaminate from the substrate. Once delaminated, it finally cracks under the repetitive loads and the coating gets stripped off with debris remaining in the wear track, which shows typical signs of combined abrasive and adhesive fretting wear.

To summarize, the produced coatings with a top TiO_2 layer and the mixed oxide barrier layer (Al_2TiO_5) have the potential to be a multifunctional coating with TiO_2 (anatase) as a good photocatalyst. Unfortunately, the anatase content of the coatings produced in the standard electrolyte is quite low and there seems to be not much potential for increasing the content dramatically. Adding anatase particles is a solution, but suffers from two drawbacks which makes it difficult to control the amount and localisation of anatase within the coating. There is first the polymorphic transformation of the anatase phase into rutile under the discharges and second the particles do enter the coating via the open pores with the highest anatase concentration at the interface. Furthermore, only the corrosion resistance could benefit from the particle addition but the wear resistance is suffering.

In order to obtain coatings with significantly improved photocatalytic properties, short treatment times at lower voltages in anatase containing electrolytes seems to be the right way. However, thin coatings with poor wear and corrosion properties are the drawback. On the other hand, thicker coatings without anatase addition could solve the problem of wear and corrosion resistance, but photoactivity is supposed to be low. While particle addition is not affecting corrosion resistance, it reduces wear resistance drastically. Thus, it seems to be difficult to produce coatings, which have a good combination of all three properties.

5. Summary and conclusions

The results of the current studies suggest that:

1) PEO processing of aluminium alloys in a simple aqueous solution of 40 g/L potassium titanium-oxide oxalate dihydrate can produce TiO_2 layers on their surface.
2) A two layer structure is forming consisting of a TiO_2 top layer and an inner mixed oxide (Al_2TiO_5) barrier layer.
3) The coatings growth mechanism appears to be a combination of deposition and sintering discharges. While the early coating formation stage is a classical PEO process resulting in the mixed oxide barrier layer composed out of substrate (Al) and electrolyte components (Ti), the top TiO_2 layer growth is deposition controlled where only electrolyte components are incorporated and sintered by the discharges.
4) At least two type of discharges occur and are responsible for the coating formation. Up to 5 min treatment time, mainly discharges due to the potential difference across the coating occur, while at longer treatment times surface discharges at the edges of gas bubbles sticking at the surface become more dominant. The appearance of the second type of discharges can be correlated with a change of coating growth rate.
5) The addition of anatase particles has only minor effect on the PEO processing, but influence the coating growth rate and can affect the coating properties strongly. Generally, the corrosion resistance is improved, the photoactivity is more predictable, but the wear resistance is reduced by the particle addition.
6) It is possible to produce TiO_2 layers on aluminium alloys via PEO processing, which have the potential to combine good wear and corrosion resistance with photoactivity. Thus, they can be considered as multifunctional surfaces. However, it is difficult to control and improve all three properties at the same time.

CRediT authorship contribution statement

S. Ignjatović: Writing - original draft, Visualization. **C. Blawert:** Writing - original draft, Writing - review & editing, Methodology, Project administration. **M. Serdechnova:** Writing - review & editing, Project administration, Formal analysis, Visualization. **S. Karpushenkov:** Conceptualization, Methodology, Visualization. **M. Damjanović:** Writing - review & editing. **P. Karlova:** Investigation, Visualization. **D.C.F. Wieland:** Investigation, Writing - review & editing. **M. Starykevich:** Investigation, Visualization. **S. Stojanović:** Investigation, Visualization. **Lj. Damjanović-Vasilić:** Writing - review & editing. **M.L. Zheludkevich:** Supervision, Writing - review & editing.

Declaration of Competing Interest

The authors declare that they have no known competing financial interests or personal relationships that could have appeared to influence the work reported in this paper.

Acknowledgements

This work was partially supported by Research Executive Agency (European Commission) in frame of Horizon2020-MSCA/RISE-2018 FUNCOAT project (Grant agreement No. 823942, “Development and design of novel multiFUNctional PEO COATings”). The authors thank Anton Davydok for the experimental support within DESY beamline experiments. We also thank PETRA III (Hamburg, Germany) for granting the P03 proposal I-20190157 for localized phase composition analysis.

References

[1] A. Ayday, M. Durman, Growth characteristics of plasma electrolytic oxidation coatings on aluminum alloys, Acta Phys. Pol. A 127 (4) (2015) 886–887.
[2] E. Matykina, R. Arrabal, P. Skeldon, G.E. Thompson, Investigation of the growth processes of coatings formed by AC plasma electrolytic oxidation of aluminium, Electrochim. Acta 54 (27) (2009) 6767–6778.
[3] M. Montazeri, C. Dehghanian, M. Shokouhfar, A. Baradaran, Investigation of the voltage and time effects on the formation of hydroxyapatite-containing titania prepared by plasma electrolytic oxidation on Ti–6Al–4V alloy and its corrosion behaviour, Appl. Surf. Sci. 257 (2011) 7268–7275.
[4] X. Liu, G. Li, Y. Xia, Investigation of the discharge mechanism of plasma electrolytic oxidation using Ti tracer, Surf. Coat. Technol. 206 (21) (2012) 4462–4465.
[5] M. Javidi, H. Fadaee, Plasma electrolytic oxidation of 2024–T3 aluminum alloy and investigation on microstructure and wear behaviour, Appl. Surf. Sci. 286 (2013) 212–219.
[6] R.O. Hussein, X. Nie, D.O. Northwood, An investigation of ceramic coating growth mechanisms in plasma electrolytic oxidation (PEO) processing, Electrochim. Acta 112 (2013) 111–119.
[7] A.L. Yerokhin, L.O. Snizhko, N.L. Gurevina, A. Leyland, A. Pilkington, A. Matthews, Discharge characterization in plasma electrolytic oxidation of aluminium, J.Phys. D: Appl. Phys. 36 (17) (2003) 2110–2120. PII: S0022-3727 (03) 61431-2.
[8] C. Blawert, M.L. Zheludkevich, M. Mohedano, X. Lu, Plasma Electrolytic Oxidation (PEO) of Metals and Alloys, Encyclopedia Interfacial Chem. (2018) 423–438. https://www.sciencedirect.com/science/article/pii/B9780124095472133980?via%3Dihub.
[9] S.V. Oleinik, V.S. Rudnev, Y.A. Kuzenkov, T.P. Yarovaya, L.F. Trubetskaya, P. M. Nedozorov, Corrosion inhibitors in PEO-coatings on aluminum alloys, Prot. Met. Phys. Chem. Surf. 50 (7) (2014) 893–897.
[10] S.V. Oleinik, V.S. Rudnev, A.Y. Kuzenkov, T.P. Yarovaya, L.F. Trubetskaya, P. M. Nedozorov, Modification of plasma electrolytic coatings on aluminum alloys with corrosion inhibitors, Prot. Met. Phys. Chem. Surf. 49 (7) (2013) 885–890.
[11] P.S. Gordienko, V.S. Rudnev, Electrochemical Formation of Coatings on Aluminum and its Alloys at Spark and Breakdown Potentials), Dal’nauka, Vladivostok, 1999.
[12] V.S. Rudnev, Multiphase anodic layers and prospects of their application, Prot. Met. Phys. Chem. Surf. 44 (3) (2008) 263–272.
[13] Lord Famiyeh, Xiaohu Huang - Plasma Electrolytic Oxidation Coatings on Aluminum Alloys Microstructures, Properties, and Applications. Mod Concept Material Sci. 2(1) (2019). MCMS.MS.ID.000526.
[14] A.L. Yerokhin, A. Shatrov, V. Samsonov, P. Shashkov, A. Pilkington, A. Leyland, A. Matthews, Oxide ceramic coatings on aluminium alloys produced by a pulsed bipolar plasma electrolytic oxidation process, Surf. Coat. Technol. 199 (2-3) (2005) 150–157.
[15] R.O. Hussein, X. Nie, D.O. Northwood, Influence of process parameters on electrolytic plasma discharging behaviour and aluminum oxide coating microstructure, Surf. Coat. Technol. 205 (6) (2010) 1659–1667.
[16] G. Sundararajan, L. Rama Krishna, Mechanisms underlying the formation of thick alumina coatings through the MAO coating technology, Surf. Coat. Technol. 167 (2-3) (2003) 269–277.
[17] R.O. Hussein, D.O. Northwood, X. Nie, The effect of processing parameters and substrate composition on the corrosion resistance of plasma electrolytic oxidation (PEO) coated magnesium alloys, Surf. Coat. Technol. 237 (2013) 357–368.
[18] R. Arrabal, E. Matykina, T. Hashimoto, P. Skeldon, G.E. Thompson, Characterization of AC PEO coatings on magnesium alloys, Surf. Coat. Technol. 203 (16) (2009) 2207–2220.
[19] N. Godja, N. Kiss, C.h. Löcker, A. Schindel, A. Gavrilovic, J. Wosik, R. Mann, J. Wendrinsky, A. Merstallinger, G.E. Nauer, Preparation and characterization of spark-anodized Al-alloys: physical, chemical and tribological properties, Tribol. Int. 43 (7) (2010) 1253–1261.
[20] E. Matykina, R. Arrabal, A. Mohamed, P. Skeldon, G.E. Thompson, Plasma electrolytic oxidation of pre-anodized aluminium, Corros. Sci. 51 (12) (2009) 2897–2905.
[21] M. Treviño, N.F. Garza-Montes-de-Oca, A. Pérez, M.A.L. Hernández-Rodríguez, A. Juárez, R. Colás, Wear of an aluminium alloy coated by plasma electrolytic oxidation, Surf. Coat. Technol. 206 (8-9) (2012) 2213–2219.
[22] A. Venugopal, J. Srinath, L. Rama Krishna, P. Ramesh Narayanan, S.C. Sharma, P. V. Venkitakrishnan, Corrosion and nanomechanical behaviours of plasma electrolytic oxidation coated AA7020-T6 aluminum alloy, Mater. Sci. Eng. A 660 (2016) 39–46.
[23] V. Dehnavi, D.W. Shoesmith, B.L. Luan, M. Yari, X.Y. Liu, S. Rohani, Corrosion properties of plasma electrolytic oxidation coatings on an aluminium alloy e The effect of the PEO process stage, Mater. Chem. Phys. 161 (2015) 49-58.
[24] R.O. Hussein, D.O. Northwood, Production of anti-corrosion coatings on light alloys (Al, Mg, Ti) by plasma-electrolytic oxidation (PEO), (2014) chapter 11, pp. 202-238.
[25] L. Rama Krishna, K.R.C. Somaraju, G. Sundararajan, The tribological performance of ultra-hard ceramic composite coatings obtained through microarc oxidation, Surf. Coat. Technol. 163-164 (2003) 484–490.
[26] X. Nie, E.I. Meletis, J.C. Jiang, A. Leyland, A.L. Yerokhin, A. Matthews, Abrasive wear/corrosion properties and TEM analysis of Al_2O_3 coatings fabricated using plasma electrolysis, Surf. Coat. Technol. 149 (2-3) (2002) 245–251.
[27] S. Stojadinović, N. Radić, R. Vasilić, M. Petković, P. Stefanov, L.j. Zeković, B. Grbić, Photocatalytic properties of TiO2/WO3 coatings formed by plasma electrolytic oxidation of titanium in 12-tungstosilicic acid, Appl. Catal. B 126 (2012) 334–341.
[28] A. Fujishima, X. Zhang, D. Tryk, TiO2 photocatalysis and related surface phenomena, Surf. Sci. Rep. 63 (12) (2008) 515–582.
[29] L.K. Mirelman, J.A. Curran, T.W. Clyne, The production of anatase-rich photoactive coatings by plasma electrolytic oxidation, Surf. Coat. Technol. 207 (2012) 66–71.
[30] N. Tadić, S. Stojadinović, N. Radić, B. Grbić, R. Vasilić, Characterization and photocatalytic properties of tungsten doped TiO 2 coatings on aluminum obtained by plasma electrolytic oxidation, Surf. Coat. Technol. 305 (2016) 192–199.

[31] S. Franz, D. Perego, O. Marchese, A. Lucotti, M. Bestetti, Photoactive TiO2 coatings obtained by Plasma Electrolytic Oxidation in refrigerated electrolytes, Appl. Surf. Sci. 385 (2016) 498–505.
[32] L. Liu, H. Zhao, J.M. Andino, Y. Li, Photocatalytic CO2 reduction with H2O on TiO2 nanocrystals: comparison of anatase, rutile, and brookite polymorphs and exploration of surface chemistry, ACS Catal. 2 (8) (2012) 1817–1828.
[33] D.A.H. Hanaor, C.C. Sorrell, Review of the anatase to rutile phase transformation, J. Mater. Sci. 46 (4) (2011) 855–874.
[34] D. Krupa, J. Baszkiewicz, J. Zdunek, J. Smolik, Z. Słomka, J.W. Sobczak, Characterization of the surface layers formed on titanium by plasma electrolytic oxidation, Surf. Coat. Technol. 205 (6) (2010) 1743–1749.
[35] J. He, Q.Z. Cai, Y.G. Ji, H.H. Luo, D.J. Li, B. Yu, Influence of fluorine on the structure and photocatalytic activity of TiO2 film prepared in tungstate-electrolyte via micro-arc oxidation, J. Alloy. Compd. 482 (1-2) (2009) 476–481.
[36] X. Nie, A. Leyland, A. Matthews, Deposition of layered bioceramic hydroxyapatite/TiO2 coatings on titanium alloys using a hybrid technique of micro-arc oxidation and electrophoresisSurf. Coat.Technol. 125 (2000) 407-414. PII: S0257-8972 (99) 00612-X.
[37] A.L. Yerokhin, X. Nie, A. Leyland, A. Matthews, Characterisation of oxide films produced by plasma electrolytic oxidation of a Ti-6Al-4V alloy, Surf. Coat. Technol. 130 (2000) 195-206. PII: S0257-8972 (00) 00719-2.
[38] D. Dzhurinskiy, Y. Gao, W.-K. Yeung, E. Strumban, V. Leshchinsky, P.-J. Chu, A. Matthews, A. Yerokhin, R.G. Maev, Characterization and corrosion evaluation of TiO2:n-HA coatings on titanium alloy formed by plasma electrolytic oxidation, Surf. Coat. Technol. 269 (2015) 258–265.
[39] Franz, S., et al., Exploiting Direct Current Plasma Electrolytic Oxidation to Boost Photoelectrocatalysis, Catalysts 10 (2020) 325.
[40] A.L. Yerokhin, A.A. Voevodin, V.V. Lyubimov, J. Zabinski, M.Donley, Plasma electrolytic fabrication of oxide ceramic surface layers for tribotechnical purpose on aluminium alloys, Surf. Coat. Technol. 110 (1998) 140–146. PII S0257-8972 (98) 00694-X.
[41] A. Bahramian, K. Raeissi, A. Hakimizad, An investigation of the characteristics of Al2O3/TiO2 PEO nanocomposite coating, Appl. Surf. Sci. 351 (2015) 13–26.
[42] P. Angerer, et al., Titanium oxide layers on aluminium substrates produced by the anodic spark deposition process, Mater. Chem. Phys. 128 (1) (2011) 28–31.
[43] S.A. Karpushenkov, Micro-plasma electrochemical formation of composite coatings on metals surface, PhD thesis defended in 2010 at Belarussian State University (Minsk, Belarus), УДК 541.13:620.197.
[44] B.K. Sharma, Instrumental methods of chemical analysis, Krishna Prakashan Media (P) Ltd, 2015.
[45] L.i. Wang, L.i. Chen, Z. Yan, W. Fu, Optical emission spectroscopy studies of discharge mechanism and plasma characteristics during plasma electrolytic oxidation of magnesium in different electrolytes, Surf. Coat. Technol. 205 (6) (2010) 1651–1658.
[46] X. Yang, L. Chen, Y. Qu, R. Liu, K. Wei, W. Xue, Optical emission spectroscopy of plasma electrolytic oxidation process on 7075 aluminum alloy, Surf. Coat. Technol. 324 (2017) 18–25.
[47] C. Blawert, S.A. Karpushenkov, M. Serdechnova, L.S. Karpushenkava, M. L. Zheludkevich, Plasma electrolytic oxidation of zinc alloy in a phosphate-aluminate electrolyte, Appl. Surf. Sci. 505 (2020) 144552.
[48] C. Krywka, H. Neubauer, M. Priebe, T. Salditt, J. Keckes, A. Buffet, S.V. Roth, R. Doehrmann, M. Mueller, A two-dimensional waveguide beam for X-ray nanodiffraction, J. Appl. Crystallogr. 45 (1) (2012) 85–92.
[49] J. Kieffer, D. Karkoulis, PyFAI, a versatile library for azimuthal regrouping, J. Phys.: Conf. Ser. 425 (20) (2013) 202012.
[50] R.O. Hussein, X. Nie, D.O. Northwood, A. Yerokhin, A. Matthews, Spectroscopic study of electrolytic plasma and discharging behaviour during the plasma electrolytic oxidation (PEO) process, J. Phys. D: Appl. Phys. 43 (10) (2010) 105203.
[51] L.O. Snizhko, A.L. Yerokhin, A. Pilkington, N.L. Gurevina, D.O. Misnyankin, A. Leyland, A. Matthews, Anodic processes in plasma electrolytic oxidation of aluminium in alkaline solutions, Electrochim. Acta 49 (13) (2004) 2085–2095.
[52] A.G. Rakoch, E.P. Monakhova, Z.V. Khabibullina, M. Serdechnova, C. Blawert, M. L. Zheludkevich, A.A. Gladkova, Plasma electrolytic oxidation of AZ31 and AZ91 magnesium alloys: comparison of coatings formation mechanism, J. Magnesium Alloys 8 (3) (2020) 587–600.
[53] Y. Chen, X. Lu, C. Blawert, M.L. Zheludkevich, T. Zhang, F. Wang, Formation of self-lubricating PEO coating via in-situ incorporation of PTFE particles, Surf. Coat. Technol. 337 (2018) 379–388.
[54] RUFF sample data, integrated database of Raman spectra, X-ray diffraction and chemistry data for minerals. https://rruff.info/Rutile/R060745 (accessed at 20.07.2020).
[55] RUFF sample data, integrated database of Raman spectra, X-ray diffraction and chemistry data for minerals. https://rruff.info/Anatase/R060277 (accessed at 20.07.2020).
[56] D.L. Liao, G.S. Wu, B.Q. Liao, Zeta potential of shape-controlled TiO2 nanoparticles with surfactants, Colloids Surf., A 348 (1-3) (2009) 270–275.
[57] Y. Rodriguez-Jaimes, D.I. Naranjo, S. Blanco, S.J. García-Vergara, Formation of Ca/P ceramic coatings by Plasma Electrolytic Oxidation (PEO) on Ti6Al4V ELI alloy, J. Phys.: Conf. Ser. 935 (2017) 012031.
[58] P. Bala Srinivasan, J. Liang, C. Blawert, M. Störmer, W. Dietzel, Effect of current density on the microstructure and corrosion behaviour of plasma electrolytic oxidation treated AM50 magnesium alloy, Appl. Surf. Sci. 255 (7) (2009) 4212–4218.
[59] J. Xu, F.u. Liu, J. Luo, L. Zhao, Effects of anodic voltages on microstructure and properties of plasma electrolytic oxidation coatings on biomedical NiTi alloy, J. Mater. Sci. Technol. 29 (1) (2013) 22–28.
[60] W. Zhu, Y.-J. Fang, H. Zheng, G. Tan, H. Cheng, C. Ning, Effect of applied voltage on phase components of composite coatings prepared by micro-arc oxidation, Thin Solid Films 544 (2013) 79–82.
[61] G. Rapheal, S. Kumar, N. Scharnagl, C. Blawert, Effect of current density on the microstructure and corrosion properties of plasma electrolytic oxidation (PEO) coatings on AM50 Mg alloy produced in an electrolyte containing clay additives, Surf. Coat. Technol. 289 (2016) 150–164.
[62] Y. Gao, A. Yerokhin, A. Matthews, Effect of current mode on PEO treatment of magnesium in Ca- and P-containing electrolyte and resulting coatings, Appl. Surf. Sci. 316 (2014) 558–567.
[63] E. Akbari, F. Di Franco, P. Ceraolo, K. Raeissi, M. Santamaria, A. Hakimizad, Electrochemically-induced TiO_2 incorporation for enhancing corrosion and tribocorrosion resistance of PEO coating on 7075 Al alloy, Corros. Sci. 143 (2018) 314–328.